Title: Individualized fMRI neuromodulation enhances swallow and tongue motor and sensory control: an intervention targeted for radiation-induced cranial neuropathy following head and neck cancer.

Papageorgiou, T.D.[1-4,6-8], Webb, J. [1,2]*, Allam A. [1,2]*, Froudarakis, E. [5,9], Rohren, E.M.[12], Sturgis, E.M.[10], Hutcheson K.[11], Heilbronner, S.R.[2,13]
1 Department of Psychiatry, Baylor College of Medicine, Houston, U.S.A.
2 Department of Neuroscience, Baylor College of Medicine, Houston, U.S.A.
3 Department of Physical Medicine & Rehabilitation, Baylor College of Medicine, Houston, U.S.A.
4 School of Medicine, Baylor College of Medicine, Houston, U.S.A.
5 School of Medicine, Crete, Greece
6 Department of Electrical and Computer Engineering, Rice University, Houston, U.S.A.
7 Center for Space Medicine, Baylor College of Medicine, Houston, U.S.A.
8 Dan L. Duncan Comprehensive Cancer Center, Baylor College of Medicine, Houston, U.S.A.
9 Institute of Molecular Biology and Biotechnology, FORTH, Heraklion, Greece
10 Department of Otolaryngology – Head and Neck Surgery, Baylor College of Medicine, Houston, U.S.A.
11. Department of Head and Neck Surgery, M.D. Anderson Cancer Center, Houston, U.S.A.
12. Department of Radiology, Baylor College of Medicine, Houston, U.S.A.
13. Department of Neurosurgery, Baylor College of Medicine, Houston, U.S.A.
* equal contribution
To whom correspondence should be addressed. E-mail: T.Dorina.Papageorgiou@bcm.edu

Sources of Support: This study is funded by grants to T.D. Papageorgiou: McNair Medical Institute, Robert and Janice McNair Foundation, Mission Connect, IP Award The Institute of Rehabilitation Research, Center for Alzheimer's and Neurodegenerative Disease, Jan and Dan Duncan Neurological Research Institute, Naman Basic Science Faculty Award, Fight for Sight, NIH-T32, NEI; NIH-T32, NINDS.

Author contributions: T.D.P. conceptualized, designed research, and synthesized findings; T.D.P, performed study experiments; T.D.P., W.J., A.A., R.H., and E.F. contributed analytic tools; J.W., A.A., T.D.P. analyzed data; T.D.P., J.W., A.A., K.H., E.M.R., S.R.H., E.M.S. interpreted findings; T.D.P. wrote the paper.

Disclosures
T. D. Papageorgiou: pending patent applications: U.S. Patent Application No.: 16/954,256; European Patent No. 19 753 851.5, WIPO Publication No. WO 2019/160754

Abstract
Introduction: Adequate sensory inputs and motor control are essential components of safe swallowing, with significant impact on both quality of life and patient survival. Conversely, both of these neuronal activities are negatively impacted during the early phases of ALS development, following instrumentation of the cervical spine through an anterior approach and broadly by delivery of surgical and radiation-based treatments for head and neck cancer. Our goal is to demonstrate the feasibility, and preliminary efficacy of the individualized fMRI neuromodulation (iNM) intervention pioneered by the Papageorgiou Lab (U.S. Patent No.16/954,256; European Patent No. 19 753 851.5) in enhancing tongue motor and sensory control (TMSC) in these variable patient populations. Although clinical trials show that steroids (NCT04151082) and gabapentin (NCT03747562) temporarily reduce pain, their adverse effects compromise tolerance and adherence. Thus, we need new treatments. The goal here was to strengthen networks that regulate TMSC through our individualized fMRI AI-NeuroModulation, termed iNM fMRI measures the magnitude and spatial extent of the ratio of oxygenated (O2) to deoxygenated hemoglobin (Hb). Our non-invasive, precision-medicine AI-iNM intervention: (1) target primary motor and sensory areas in the brain that regulate swallowing with 1mm level precision, (2) targets each patient's unique anatomical motor and sensory extents , and (3) iNM is and are guided by reinforcing or inhibiting the HbO2 intensity and extent of each patient's unique brain network, as opposed to self-regulation of the HbO2 intensity.

Methods: Thirty healthy subjects participated in a 2-day study which included iNM and control conditions. We first computed the individualized TMSC cortical selectivity to be targeted in the iNM condition. Support vector machine (SVM) classified cortical tongue direction and tongue-at-rest patterns generated via iNM and control. We quantified the BOLD magnitude for each network by computing the area under the curve (AUC), variance and association between brain states and TMSC responses via dynamic causal modeling (DCM).

Results: The mechanisms associated with attention-memory and sensorimotor iNM are: 1. 45% increase in the AUC's BOLD magnitude ($p<0.001$); 2. 14% decrease in the BOLD's intensity variance ($p<0.01$); and 3. 20% increase in network expansion ($p<0.001$). DCM uncovered 97% of the trials as pure motor signal, while 3% were noise in the iNM condition (compared to 83% of the TMSC trials and 17% noise in the control condition): 1. 70% motor-to-motor (M1, motor cerebellum, basal ganglia) and 70% motor-to-sensory; 2. 69% sensory-to-sensory (intraparietal lobule, insula, claustrum, sensory cerebellum, ACC); and 3. 70% sensorimotor-to-attention-memory network connectivities.

Conclusion: iNM showed spatiotemporal causality between networks that regulate motor and sensory control, which can serve as clinical biomarkers for the RICN alleviation in head and neck cancer survivors.

Introduction

Neuromodulation, which encompasses a range of therapies ranging from invasive deep brain stimulation procedures, to non-invasive, such a transcranial magnetic stimulation (TMS), transcutaneous electrical nerve stimulation (TENS), and fMRI neurofeedback interventions, is an expanding field in precision medicine. These interventions, defined by their ability to modulate neural activity, are employed to treat psychiatric, neurologic, and in general pathologic conditions like chronic pain.[1–6] This study presents the application of guided, individualized fMRI neurofeedback by targeting each participant's unique anatomical and functional networks, which we call individualized real-time fMRI closed-loop Neuromodulation (iNM).

Our precision medicine intervention differs from other non-invasive approaches, such as fMRI neurofeedback or TMS in the following ways: (1) it is not anatomically limited, targeting only one cortical area at a time, as it can target each patient's unique cortical and subcortical anatomy with 1mm precision; (2) it is individualized at both the anatomical and functional levels; (3) it can target subcortical networks - unlike TMS - with 1mm resolution-precision that correspond to tongue motor and sensory control (TMSC); (4) it is regulated/guided spatiotemporally as opposed to the sole self-regulation of cortical and subcortical areas involved in the pathological response we aim to neuromodulate. It extracts maximum or minimum time-resolved signal intensity segments obtained under control conditions and reinforces (i.e., motor network signal) or inhibits (i.e., pain network signal) these specific signals; i.e., the physiologic response threshold is increased to further activate the networks we aim to neuromodulate. (5) iNM is adaptive, as each patient's cortical motor and sensory network inputs and outputs regulating swallowing and TMSC evolve over time to achieve bilateral network activation, similar to a healthy state (**Fig. 1**). Thus, *it is important to provide an intervention that can access the entire brain but also individualized to successfully manage symptoms, which are unique to each patient based on the lower cranial nerve branches lesioned following radiation, afferent or efferent nerves lesioned, and brain networks involved*.

The main objective of this study was to investigate the potential for modifying motor and sensory networks associated with the interoceptive response of tongue mobility through iNM. The principle of iNM is that it bypasses lesioned neural pathways and capitalizes on strengthening others that are intact to become functionally associated to the lesioned ones. Defined as both a conscious and subconscious process in which the nervous system exhibits a capacity for sensing and incorporating internal bodily signals to form and represent momentary internal states, interoception can be displayed through various functions. Our long-term goal is to provide an efficacious treatment for neuropathologies affecting the regulation of sensorimotor control of the tongue during swallowing (sequential activation of the tongue, pharyngeal and laryngeal muscles), an interoceptive function which can be impacted by neuropathic pain, another type of interoception.[7–14] TMSC, essential for speech production, swallowing, and mastication functions is controlled by the glossopharyngeal (CNIX), vagus (CNX), and hypoglossal (CNXII) lower cranial nerves, which receive projections from sensory (BA 3/1/2) and motor (BA 4/6) areas. Neuropathic pain symptoms along lower cranial nerve paths such as the neck, jaw, and oral cavity can emerge following radiation treatment for head and neck cancers (HNC) like oropharyngeal cancer (OPC), referred to as radiation-induced cranial neuropathy (RICN).[15–20]

TMSC can also arise after surgical interventions, such as anterior cervical discectomy and fusion, which can safely and effectively treat cervical disc herniation with a success rate of 70%.[21,22] ACDF, albeit a common procedure, comprising 80% of cervical spinal surgeries it can result in complications, including esophageal perforation, recurrent laryngeal nerve palsy, dyspnea, dysphonia.[23–32] One of the most common adverse sequelae following ACDF is dysphagia with 34%–38% of patients reporting this symptom within 2 weeks post-surgery, and 25.5% of patients experiencing persistent and debilitating dysphagia 1-year postoperatively, which can cause ***tongue muscle atrophy and loss of tongue strength***.[33–44] This sequalae impacts quality of life and can even result in mortality due to aspiration and pneumonia.[46] While significant increases in annual ACDF-associated dysphagia rates have been reported, indicating an urgent need to manage ACDF-related adverse outcomes, treatments are lacking, as current pharmacotherapies, such as steroids are associated with poor

tolerance and adherence. [47–52] Additionally, tracheal traction or pharyngeal movement exercises, modified diets, and laryngeal rehabilitation therapy, have had limited success.[53–57]

iNM treatment can also be impactful in alleviating other neuropathies through the strengthening of cortical and subcortical motor networks and inhibiting pain networks that regulate arm motor control and strength in breast cancer (BCA) patients, following lymph node dissection dissection, which is part of the diagnosis and treatment of one of the most commonly occurring malignancies in women, as 1 in 8 will develop invasive BCA in their lifetime.[58–62] Based on the CONCORD-2 study, although 85% of BCA patients live >5 years due to improved cancer treatment, 20-60% of them develop chronic post-mastectomy pain syndrome (PMPS) .[58–60,63–65] Most common contributors of this chronic neuropathy on the anterior thorax, axilla, shoulder, and upper arm/shoulder motor dysfunction include surgery in the axilla, which can cause adhesions and hematomas of the intercostobrachial nerve, or radiotherapy.[66–68] This debilitating pain affects inspiration, expiration, and movement of the trunk, thereby affecting physical and mental health, as 25% of women with PMPS report severe depression, and 54% report changes in employment, and an inability to seek medical care, as they experience physical, psychosocial, and social ramifications.[66–75] Thus, the space for a non-invasive and safe treatment is apparent, as physical therapy, hypnosedation, myofascial, and stress management training, along with the same pharmacological agents as those used for RICN-, and ACDF-induced neuropathy, which fail to alleviate PMPS due to drug-drug interactions, and drug-induced side-effects.[76–79]

Tongue motor control changes can occur bilaterally and symmetrically (fig. SI-6as in our patient who underwent iNM. About 48% of RICN patients experience speech dysarthria and dysphonia, dysphagia (swallowing) and mastication difficulties, progression of dental disease, loss of taste sensation in the tongue.[15,20,80,81] Further, according to the CDC, 18,917 cases of OPC arose as a result of human papilloma virus (HPV), with a high incidence rate of 82% in males while the number of cervical carcinoma cases were 11,788 for which a vaccine is available while for OPC-HPV there is not yet, one.[82–85] Despite high prevalence, RICN remains inadequately addressed by current treatment and intervention efforts and greatly impairs quality of life. Routine care consists of corticosteroids, opioids, anti-epileptics, and tricyclic antidepressants, which often become intolerable due to drug interactions and side effects.[86,87] Thus, the need for new, non-invasive, and safe treatments is apparent. The present study aimed to demonstrate the feasibility of and discover the causal mechanisms underlying the use of iNM to neuromodulate TMSC networks that regulate tongue movement and sensation.

Unfortunately, the mechanism of RICN is poorly understood. Radiation results in necrosis of cancer cells but can also induce necrosis to adjacent normal cells, as a consequence of cytokine release and inflammatory factors, which in turn can cause perineural fibrosis, followed by atrophy, vessel and nerve ulceration, and consequently nerve damage.[88] This cascade of inflammatory factors affects not only the tongue tissue and muscles, but can also lead to structural and functional changes in motor and sensory pathways controlling tongue movement and swallowing causing neuropathic pain.[89,90] This phenomenon worsens the long-term RICN patients' quality of life and rehabilitation prognosis. When pain becomes chronic, nociceptive pain fibers activate and begin modulating the activity of motor and sensory areas. Chronic pain can lead to a sensitization phenomenon called "smudging" in the motor and sensory areas regulating tongue movement. Affected regions will blur and diffuse with neighboring or functionally related neurons in the brain. Chronic pain makes the cortical representation of that body part – in this case the tongue - less distinct, and explains why tongue motor control can become difficult to use and overly sensitized.

Here, we target neocortical tongue-specific motor and sensory regions using our individualized iNM approach. The rationale for targeting motor and sensory cortical areas that control tongue movement is two-fold: 1. RICN symptoms affect the strength and motor control of the tongue, resulting in prolonged oral transit times and persistent oral residues, reduced tongue elevation, closure, and base posterior motion; and 2. Neuropathic pain alleviation is achievable through stimulation of motor cortical areas, though not without identifiable drawbacks.[1–3,56,91–101] The clinical and physiological effectiveness of electrical stimulation methods, such as neuromuscular electrical stimulation (NMES) and transcutaneuous electrical nerve stimulation (TENS), in improving tongue muscle recruitment and swallow function for radiation-induced injuries is controversial, as it is limited in targeting irradiated tissue of the deep location of affected swallowing muscles and conflicting roles of surface musculature during swallowing.[4,102–108]

The <u>principle of our iNM intervention</u> is based on strengthening brain motor and sensory networks with the goal to strengthen tongue atrophy and LCN-innervated areas. iNM induces changes to the BOLD magnitude and spatial extent – the ratio of oxygenated to deoxygenated hemoglobin - in response to TMSC. Thus, iNM reinforces a new network to learn to control tongue movement and direction. The key to modulating the HbO2 magnitude and extent successfully is based

on the delineation of each patient's individualized anatomy and physiological dynamics that regulate TMSC, prior to the intervention (fig. 2).

The immediate goals of this study were to (1) demonstrate the feasibility of iNM in its guided regulation of interoception, specifically, targeting TMSC areas and (2) to understand the spatiotemporal causal mechanisms of the iNM intervention. We hypothesized that iNM will induce greater consistency in brain TMSC-associated patterns, as well as greater HbO2 signal-to-noise ratio (SNR).[109] To elucidate the causal mechanisms of iNM, we quantified our findings by computing: 1. Classification accuracies using support vector machine (SVM) analysis 2. The intensity and variance of the HbO2, spatiotemporally, using the sensitivity index and the area under the curve - the latter a measure that assesses the HbO2 curve over the duration of the signal in key TMS brain regions. Further, we elucidate causality between the association of dominant brain states (true signal) and the physiological response of TMSC under iNM compared to the control condition using an autoregressive hidden Markov model (AHMM) developed for eCOG data.[110] iNM introduces a biomarker-driven intervention for strengthening motor and sensory brain networks for the clinical application in RICN to alleviate oral neuropathic pain.

Materials and Methods

Subjects

Thirty healthy, right-handed volunteers (19 males, 11 females, age range = 25.37±5.56) were recruited in this 2-day study after proper informed consent was given in accordance with the Institutional Research Board of Baylor College of Medicine. Exclusion criteria included prior and current medical or psychiatric diagnoses, intake of any medications and general contraindications against MRI examinations. Participants had normal or corrected-to-normal visual acuity with MR-compatible glasses. At the end of each scanning session, the subjects received compensation for volunteering their time.

MRI and fMRI Pulse Sequence Parameters

Structural and functional brain imaging was performed at the Core for Advanced Magnetic Resonance Imaging (aka CAMRI), Baylor College of Medicine, Houston, Texas using a 3.0 T Siemens Prisma (Siemens, Erlangen, Germany). We used a 20-channel head/neck receiver-array coil for image acquisition. T1-weighted 3D magnetization-prepared gradient-echo (MPRAGE) sequence acquired 192 high-resolution axial slices (field-of-view (FOV) = 245x245 mm²; base resolution = 256x256; repetition time (TR) = 1,200ms; echo time (TE) = 2.66ms; flip angle (FA) = 12°). Functional data consisted of 33 interleaved axial slices, which were acquired using an Echo Planar Imaging (EPI) sequence (FOV = 200x200mm², voxel size = 3.1x3.1x3.0 mm, TR = 2000ms; flip angle = 90°, number of volumes = 244).

Real-time fMRI Neuromodulation Acquisition

Turbo-BrainVoyager (TBV; 2.0; Brain Innovation, Maastricht, The Netherlands; Goebel et. al., 2006) software was used to perform the following preprocessing computations on the EPI images acquired every tongue repetition (TR): (i) 3D motion correction; (ii) incremental linear detrending to remove BOLD signal drifts; (iii) display of statistical brain maps generated from a general linear model (GLM) along with beta weights (BOLD signal intensity values) for each condition; (iv) extraction of the average BOLD signal intensity values from the individualized networks acquired on Day 1 scans (see *Data Analysis*); and (v) presentation of the network's average BOLD signal intensity via the neuromodulation interface (fig. 1D). The steps of our iRTfMRI neuromodulation interface are summarized in Figure 1. To further increase our signal-to-noise ratio (SNR), we employed an exponential moving average (EMA; Cui et al., 2009) algorithm to high-pass filter the ROI's BOLD average and suppress low-frequency components of noise, such as scanner drifts, and physiological noise effects, such as heart rate and respiration. The output of the EMA was then low pass filtered via a Kalman filter to eliminate high frequency noise (Haykin SS. Kalman filtering and neural networks. Wiley Online Library; 2001). **Details on how the EMA and Kalman filter were computed can be found in the Supplemental Material section.**

Study Structure

Our study was comprised of two sessions that were separated by 5-7 days. Day 1 consisted of four functional (EPI) runs: three functional task localizer runs and one neuromodulation run. Day 2 consisted of six EPI runs: three control-no iNM runs, which alternated with three neuromodulation runs. Each EPI run was composed of 8 continuous periods that lasted for a total of 8 minutes and 12 seconds. Within each period, the subjects were cued to move their tongue in one of four directions (up; down; left; right). Each tongue movement block lasted 30secs and was interleaved with a swallow block (6 secs) and a baseline-tongue at rest block (20 secs). Direction of the movement blocks were randomly counterbalanced across runs and followed three rules: (i) each TMSC direction block occurred twice during each period; (ii) a TMSC direction block was never followed by the same TMSC direction cue; (iii) each run consisted of a unique order of blocks. **(Figure 1B)** All subjects were instructed by the PI of the study (TDP) to foster consistency in the subjects' receipt of instructions and training.

Study participants were asked to control movement of their tongue in a consistent manner: i. force of tongue movement, and ii. location of tongue's placement in the mouth. During the 30-sec tongue movement period, they were also coached to abstain from clenching their teeth, pursing their lips together, squinching their eyes, applying pressure to their cheeks, straining their facial muscles, such as those of their forehead between the eyebrows and corners of the eyes, and moving their lower jaw from any backward, forward and side to side movement. Subjects were instructed to move their tongue in the same location in their mouth by mentally assigning landmarks, such as a specific ridge on the roof of their palate or, a specific tooth for left and right movement of the tongue. A time interval was dedicated to swallow after each TMSC block. Our team was able to detect in real-time if a subject was swallowing during the TMSC task as the fMRI signal would be significantly upregulated during execution of swallow compared to TMSC task. Subjects adhered to abstinence from swallowing during the TMSC task execution and thus, we did not have to exclude swallowing from the TMSC-dedicated time series signal. During the rest block, which served as the baseline, participants stabilized their tongue between the hard and soft palate. Our instructions controlled for any confounding factors that would induce tongue motion other than the movement of the tongue, and promoted consistent TMSC so that it could be replicated in subsequent scans. Subjects were invited to participate in the fMRI and iNM experiment only if they were able to move their tongue without engaging in other facial or jaw movements.

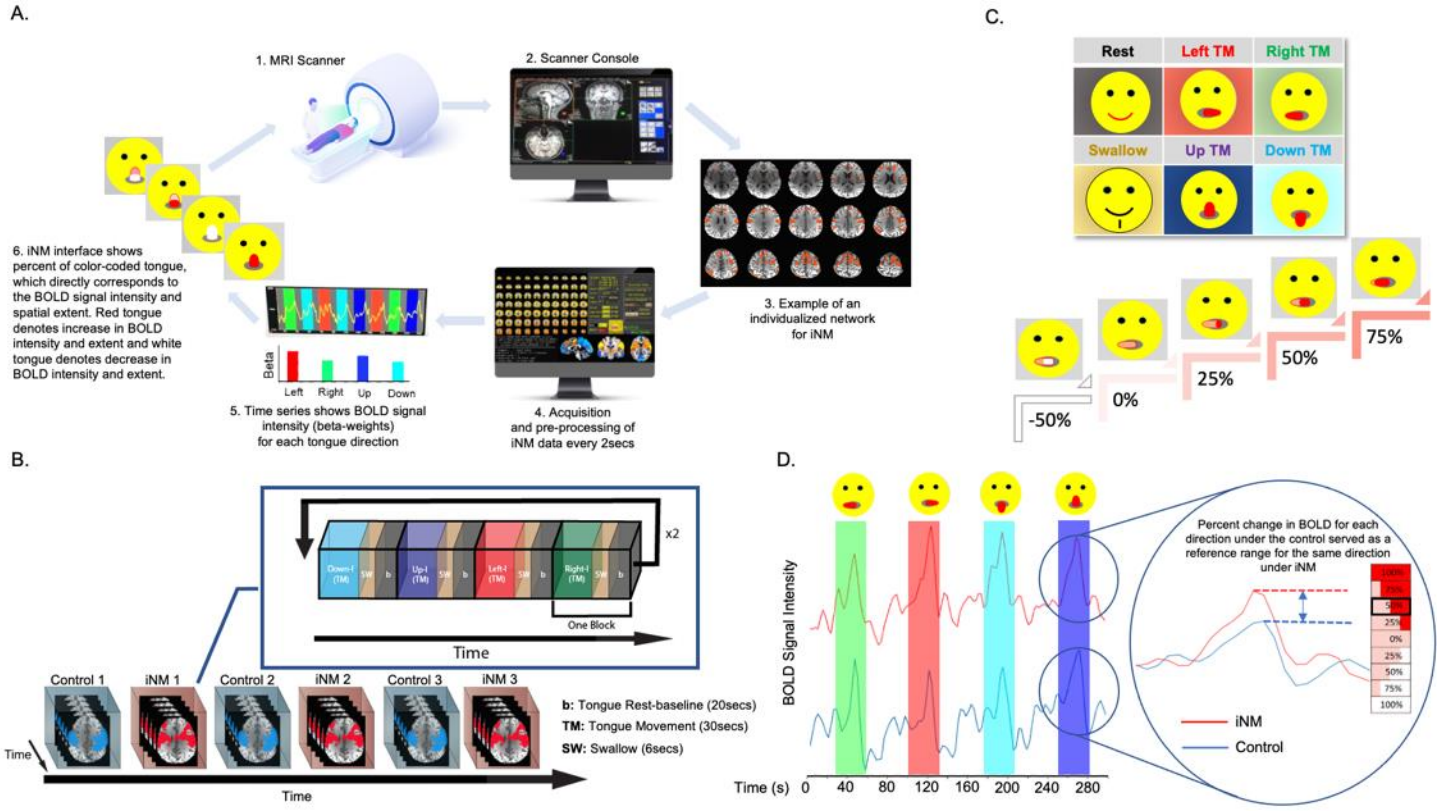

Figure 1. Individualized real-time functional MRI closed-loop neuromodulation (iNM) Intervention.
A. iNM strengthens motor and sensory control networks: 1. and 2. the MRI acquires high resolution anatomical images, which are registered to our Siemens' console computer; 3. delineate and contour each participant's individualized motor and sensory network that corresponds to tongue motor and sensory control (TMSC; left; right; up; down), as a function of the upregulated BOLD intensity and spatial extent that corresponds to each condition – cortical direction selectivity; 4. pre-process the iNM data extracted from the individualized network and apply a general linear model to decode each TMSC direction in real-time every TR=2secs (yellow line = time series, baseline - tongue at rest interval is represented with gray and TMSC red, green, blue, cyan corresponds to left, right, up, and down direction selectivity, respectively; 5. compute the BOLD signal intensity and spatial extent (individualized network) for each direction via a GLM, and the beta-weights are updated as described under 1D. 6. iNM interface shows the extent of color-coded tongue, which directly corresponds to the percent upregulation (red fill-in of the tongue) or downregulation (white fill-in of the tongue) of the BOLD signal intensity and spatial extent

B. The temporal sequence of the physiological responses, participants were asked to engage in were the same for the control-No iNM and iNM scans: each TMSC task direction block was30secs long, interleaved with 6secs-duration blocks of swallow and 20secs-duration dedicated to baseline-tongue at rest blocks. The order of tongue directions was counterbalanced across runs, and blocks cuing the same tongue direction were not stacked back-to-back.
C. iNM interface: the entire tongue was filled-in with red during control runs to motivate participants to maximally upregulate the targeted network for each tongue direction. During the iNM scans, the tongue color corresponded to the following scenarios: the BOLD magnitude and extent presents the subject's individualized brain network that regulates his/her TMSC physiology and it is presented to the participant via the emoji's tongue: 100%, 75%, 50%, 25% upregulation denoted in red fill-in of the tongue; 0% baseline denoted in pink fill-in of the tongue; -25%; -50%; -75% -100% downregulation denoted in white fill-in of the tongue.
D. Computation of the iNM signal: Percent change of the BOLD signal intensity during TMSC compared to baseline-tongue at rest during each control run served as a reference (10-th to 90-th percentile; shaded in blue) for computing the iNM signal. If the percent BOLD signal change during a 2-sec interval was higher than the 10th percentile, then the iNM interface indicated a 10% upregulation, and if it was less than the 10th percentile the iNM interface indicated downregulation.

Study Design

Overview

On Day 1, we acquired three TMSC functional localizer scans. Additionally, subjects underwent a single neuromodulation run to become acquainted with the neuromodulation interface. These localizer scans were analyzed via a GLM to delineate the individualized functional regions of interest (ROI) associated with TMSC direction selectivity during tongue movement. These individualized networks were then used to deliver neuromodulation that captured each participant's unique BOLD amplitude and spatial extent. The neuromodulation was delivered in real-time every two seconds during the tongue movement blocks. During control scans, the visual cue was always color-coded in red to motivate subjects to execute the task at maximal performance.

Computing Individualized ROIs for Neuromodulation Delivery

We acquired functional localizer scans on Day 1 to identify each participant's individualized network that controls tongue motor and sensory control. After scanning, the acquired anatomical and functional images were processed offline using AFNI (Cox, 1996; http://afni.nimh.nih.gov/afni). The anatomical data was spatially transformed to Talairach space using an average volume of 452 skull-stripped brains (TT_icbm452; www.loni.ucla.com). The functional data was preprocessed to reduce artifacts and increase SNR. Our signal pre-processing protocol included: 1. removal of outliers (head motion, physiological artifacts; 3dDespike) from the time series; 2. slice-time correction (3dTShift); 3. transformation of our oblique-acquired functional dataset to a cardinal dataset (3dWarp -oblique2card); 4. motion correction by registering each functional dataset to the first volume of the first functional run, using a 3D-rigid-body transformation; 5. spatial smoothing with a 6 mm-FWHM Gaussian kernel filter; and 6. co-registration of the functional data with the individual T1-weighted 3D-structrual data.

The three functional localizer scans acquired on Day 1 were then concatenated to increase the SNR prior to generating parametric brain maps across conditions via a General Linear Model (GLM; 3dREMLfit to adjust for temporal correlations in each voxel's time series, AFNI). The GLM included: 1. four regressors, one for each of the four TMSC directions (left; right; up; down cortical direction selectivity); 2. six covariate vectors that controlled for head motion; 3. white matter and cerebrospinal fluid means were regressed out to increase our SNR, since activity in these areas represents noise; and iv. the baseline-tongue at rest between the hard and soft palate). Each of the four regressors corresponded to each TMSC condition and was convolved with a gamma variate function, a canonical hemodynamic response function. We excluded the swallow condition from the GLM, since we did not control for the number and onset of swallows performed. We removed the first 3 TRs (6 seconds) from our rest-baseline condition to account for the lag of the hemodynamic response. Following the generation of a network of regions for tongue motor control compared to rest-baseline (voxelwise p-value=0.001 or 0.005), a cluster analysis was performed to identify highly significant ROIs (FWER<0.05) using a cluster-size of at least 50 voxels (3dClustSim, AFNI). **(Figure 2)**

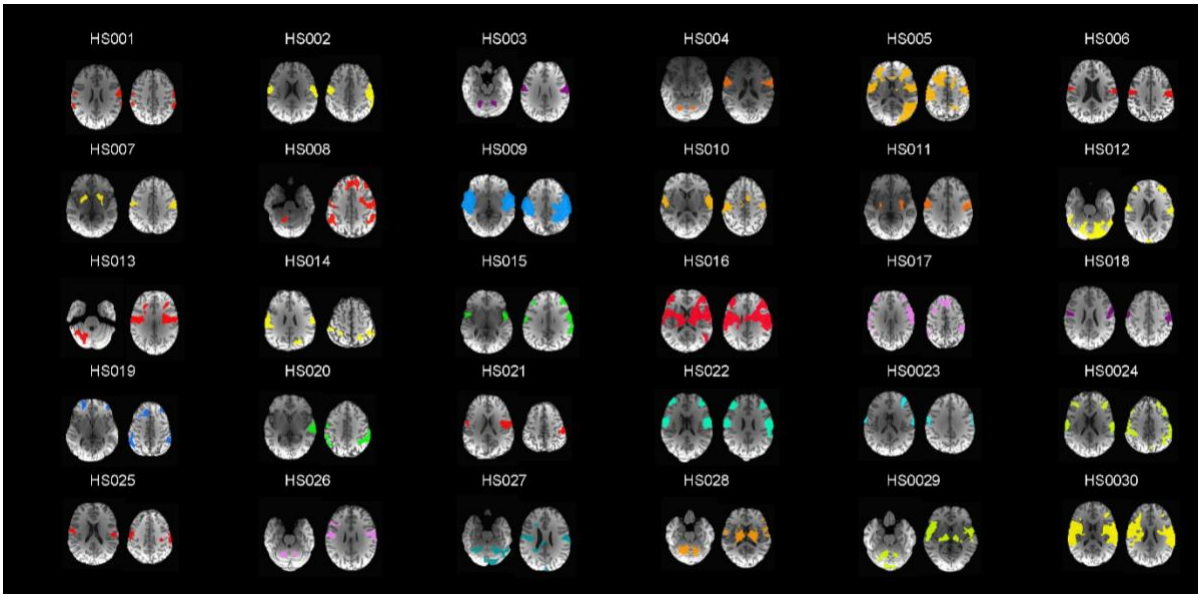

Figure 2. Individualized networks for iNM (n=30)
Optimization and efficacy of iNM is enhanced by carefully delineating the intensity and extent of the cortical network based on the patient's unique anatomy while the TIMSC physiological response is registered. Localization of TMSC is based by delineating and contouring of each patient's motor, sensory networks associated with maximal upregulation of tongue movement across directions. We find the intersection between the anatomical region and the functional intensity of each subject, while the s/he engages in TMSC prior to iNM. We then, optimize each participant's network by carefully eliminating areas that represent noise. For example, BOLD activity can extend into the cerebrospinal fluid; i.e., we carefully contour this area, if it extends over several slices or, if it does not expand spatially, we completely eliminate it.

Neuromodulation Paradigm
These individualized networks allowed us to read and deliver each participant's unique BOLD amplitude and spatial extent in the form of neuromodulation with the goal to achieve maximum upregulation of the areas that control tongue movement. **(Figure 1A)** Neuromodulation was provided via the color and extent of the emoji's tongue that was filled-in directly representing the magnitude and extent of each subject's individualized network **(Figure 1C)**. The neuromodulation signal was calculated by first acquiring the percent BOLD signal change (% BOLD PSC) generated during each control run for each TMSC direction compared to the rest block that preceded it. We computed the % BOLD PSC change from each participant's individualized areas every 2 seconds as follows:

*BOLD PSCi(j) = 100% * [ROIs BOLD during each TMSC direction i(j) –ROIs BOLD during tongue_at_rest_i(j)]/tongue_rest_i(j)*

where *i* represents each TMSC direction (left, right, up, down), *j* represents the time interval (2secs) from which the BOLD PSC of tongue motor control direction *i* was computed. The neuromodulation presented at each TR was computed by comparing the current PSC value with a PSC reference range that included 7 bins of 25% BOLD increments: -100%; -75%; -50%; -25%; 0; 25%; 50%; 75%; 100% **(Figure 1E).** During the iNM run that followed each control run, if the PSC at a given time point was within the reference range or higher than the maximum value, then the tongue was filled-in with red, which represented upregulation of the BOLD signal of the targeted ROIs that controlled a specific tongue movement **(Figure 1E)**. If the PSC though was lower than the minimal value then, the tongue was filled-in with white, and represented downregulation of the BOLD signal of the targeted ROI that controlled a specific tongue movement **(Figure 1E).**

Support Vector Machine Classification for Direction of Controlled and Voluntary Tongue Movement
Linear support vector machines (SVM) were used to decode BOLD spatial patterns of each TMSC direction generated by the 3 neuromodulation and 3 control conditions. The 3dSVM AFNI function implements a linear SVM classification where the weight vector specifies the signal direction for classification in the multivariate image space (Papageorgiou et al., 2013; Papageorgiou et al., 2009; LaConte et al., 2005).

We applied a cross-validation method for each cortical selectivity classification: 1. concatenated all TMSC directions; 2. left direction; 3. right direction; 4. up direction; 5. down direction vs. baseline-tongue at rest. For each subject, we computed classification accuracies (CAs) for the following SVM training-testing permutations by obtaining the means from a 3-fold cross-validation method: i. training and testing with control data and ii. training and testing with iNM data. **(Fig-SI 1)** We used soft margin SVMs to account for data points not linearly separable and since we found no differences in performance over a wide range of c - regularization parameter - values from 10-4 to 10+4 (geometric progression with a ratio of 10), we applied the default c=1 for all classifications to optimize training and testing errors.

SVM brain maps were generated for each TMSC direction and condition (control or iNM) as follows: a. the weight vectors corresponding to the optimal hyperplanes obtained from training each of the 3 cross-validation datasets were mapped and mean-zero standardized; b. the weight vectors generated for each subject were normalized; c. the average weight vectors across our 30 subjects were inputted into a t-test for group and cluster analyses (3dttest++ -ClustSim, AFNI); and d. t-test generated brain maps were z-scored (p= 0.005, and cluster size > 10 voxels). From the activation map for each tongue motor control direction and condition (control or iNM), we generated each cluster's local maxima (3dExtrema, AFNI). Whether more than one local maximum was generated from a cluster or, a cluster was contained within an anatomical region, only the voxels with the highest z scores which corresponded increased BOLD signal intensity were included for that region.

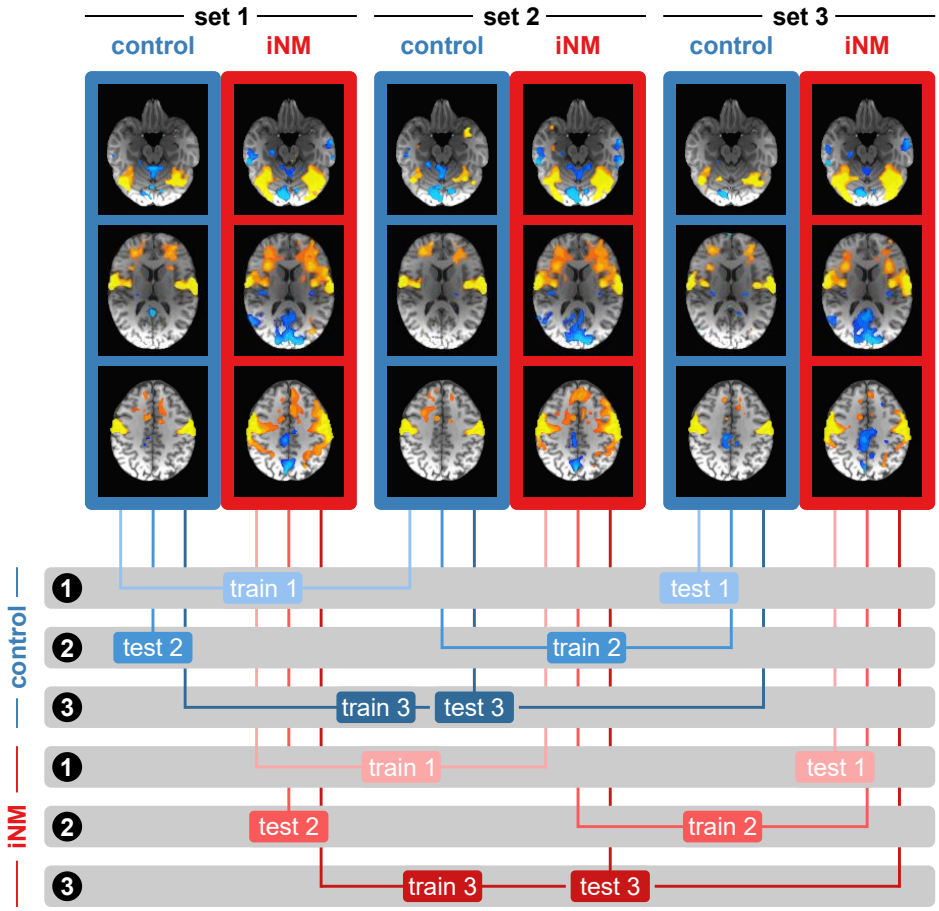

Figure SI-1. Training and testing SVM permutations using a 3-fold cross-validation design. SVM classification accuracy for each permutation was generated by computing the mean accuracies from the three corresponding test datasets.

Percent Signal Change (PSC)'s Area Under the Curve

We computed the BOLD percent signal change (PSC) for each tongue motor control direction and condition as a function of time. We categorized ROIs across motor, sensory, attention, and reward networks. The BOLD PSC time series were generated by: i. averaging the time series of voxels within an ROI; and ii. averaging over segments of signal from blocks of

the same tongue motor control direction collected from runs of the same type. Each segment of signal started from the onset of a TM block and ended at the last time point of the swallow block that followed. With each subject having 3 control and 3 iNM runs (Day 2), and each run entailing 2 blocks of TM in each direction, the PSC time series for each direction, each condition, each subject was the average over 6 segments of BOLD signal. The area under the PSC curve of each condition (control or iNM) was calculated using Simpson's Rule:

$$AUC_{con}^{reg} = \frac{1}{3}(PSC_1 + 4PSC_2 + 2PSC_3 + \cdots + 4PSC_{T-1} + PSC_T$$

Where PSCt is the PSC at the corresponding time t.
The BOLD percent signal change was then calculated using the following formula:

$$100 * (AUC_{cNMT}^{reg} - AUC_{ctrl}^{reg})/AUC_{cNMT}^{reg}$$

D' Sensitivity Index

In order to measure the strength of iNM across time and rank regions with respect to this strength, a variant of Cohen's d known as D' sensitivity index was utilized. This index quantifies the separation between the means of the control and iNM distributions with respect to their standard deviations. Assume that the fMRI data set has T time points, B blocks, S subjects, and N ROIs. Each ROI is characterized by a 3-D matrix of dimensions $T \times B \times S$. Each subject then is characterized by a 2-D matrix of dimensions $T \times B$. For a fixed time point t, let the distribution of blocks for control and iNM be $dist_{ctrl}^{s}(t)$ and $dist_{nFb}^{s}(t)$ respectively. D' for the subject s at time point t is:

$$d^{s\prime}(t) = \frac{\mu_{nFb}^{s}(\mathrm{t}) - \mu_{ctrl}^{s}(t)}{\sqrt{\frac{1}{2}(\sigma_{nFb}^{s}(t)^2 + \mu_{ctrl}^{s}(t)^2)}}, t = 1, \dots, T$$

Where $\mu_{con}^{s}(t) = mean(dist_{con}^{s}(t))$, $\sigma_{con}^{s}(t) = std(dist_{con}^{s}(t))$.
The sensitivity index between the two conditions at time point t and for the fixed region is the average sensitivity index across the subjects:

$$d'(t) = \underset{s}{\mathrm{mean}}(d^{s\prime}), s = 1, \dots, S$$

The range of d' from boostrapping of all d' time series across all ROIs for each subject was binned based on 5, 15, 25, …, 95th percentile levels. For each ROI, d'-generated score at any time point then took a value from 1 to 10 depending on which percentile d' value at that time point falls in.

Autoregressive Hidden Markov Model

To resolve dynamic latent network states during tongue movement and to validate previous results, we used an autoregressive hidden Markov model (HMM) or AHMM [3,9] on a trial-by-trial basis to identify dynamic network states exhibited by BOLD signals. Individual network states are characterized according to the patterns of directional information flow between cortical regions. More information regarding the AHMM model can be found in Pitkow's paper. For each of the 4 TM directions and each of the 2 conditions, we concatenated the blocks across subjects and generated a new data set of size N x M x T (ROIs x Trials x Time points), where M=B*S and B is the total number of the blocks (B=6) across subjects (S=30). After collapsing the 4 directions across trials we get a data set of size Nx4MxT. In the latter, there are 720 trials for each condition. On each iteration, we run HMM on data from 29 subjects (696 trials) and exclude 1 subject (leave 24 trials out). **(Figure SI-2)** The achieved distribution of AR statistics for the control condition then can be compared to those of the iNM condition. The connectivity measures within and across networks (Motor, Sensory, Attention, and Reward) were computed as the mean of the AR values between regions that comprised the respective networks.

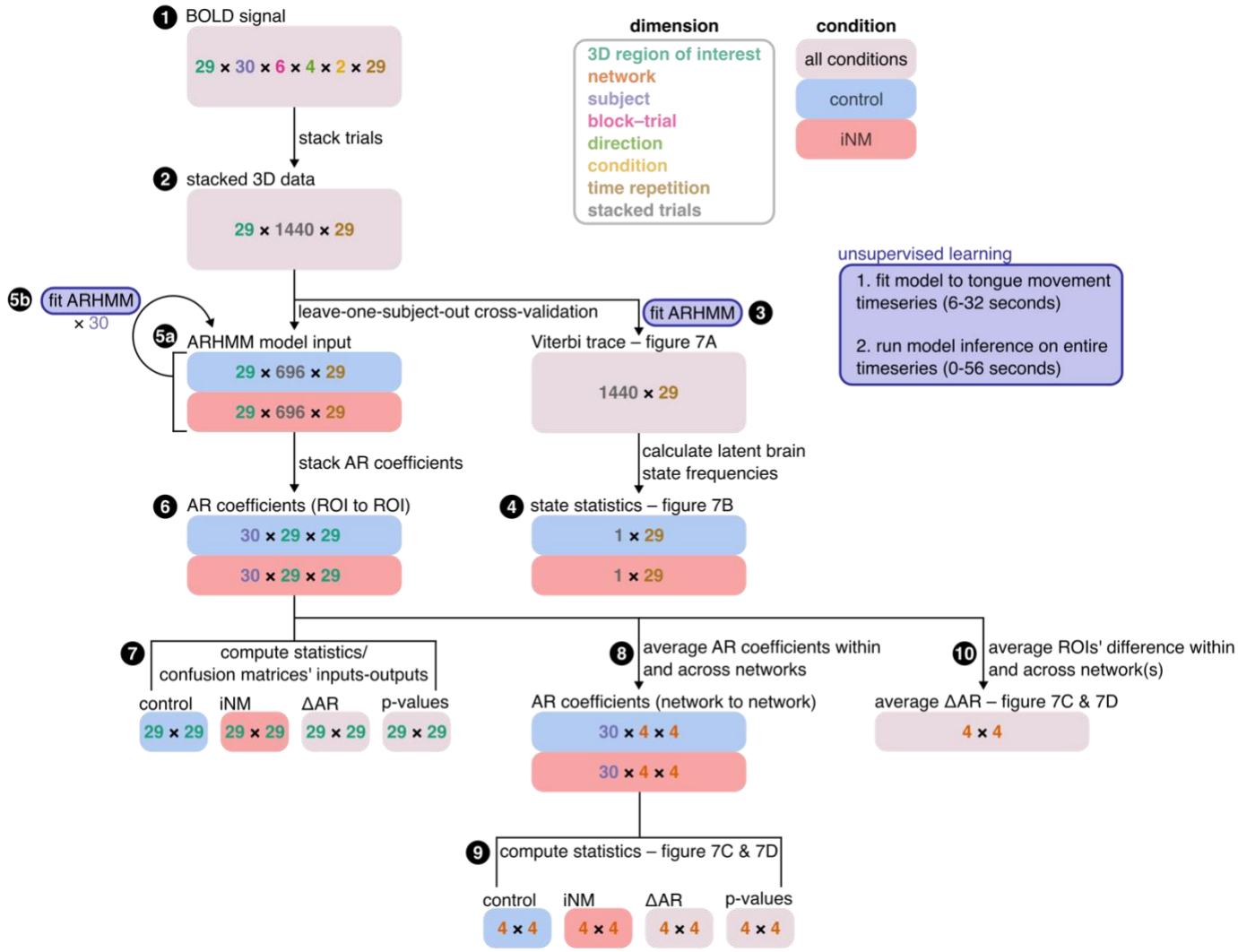

Figure SI-2: Step-by-step overview of autoregressive hidden Markov model (ARHMM) analysis. BOLD signal data (**1**) was organized by stacking trials into a single dimension (**2**) on which ARHMM analyses could be performed. The ARHMM was fit only to the timeseries corresponding to tongue movement, but model inference, via the Viterbi trace, was performed on the entire timeseries (**3** and **5**; see inset in purple box). First, the ARHMM was fit to both conditions simultaneously (**3**), and frequencies of the latent states were then calculated for trials corresponding to control and iNM conditions separately (**4**). Next, leave-one-subject-out cross-validation was performed on the stacked dataset. All trials from one subject were held out (**5a**), while ARHMM models were fit to data from the remaining twenty-nine subjects under each condition (**5b**), resulting in a total of thirty ARHMM models for both the control and iNM conditions. From the autoregressive (AR) coefficients for these models (**6**), the average confusion matrices representing connectivities between regions-of-interest (ROIs) were calculated (**7**). AR coefficients were subsequently grouped by network (**8**; i.e. motor, sensory, attention, reward), and confusion matrices representing network-to-network connectivities were similarly computed (**9**). Lastly, within each network, the sum of differences between the coefficients corresponding to control and iNM conditions were calculated (**10**).

Results

iNM Increases Consistency in the Signal Intensity and Spatial Extent Compared to the Control-no iNM Condition Using Linear Support Vector Machine Analysis

The SVM-generated cortical maps indicate voxels that are activated for a particular task compared to rest conditions. The brightness/color of the shaded voxels indicate the strength of the signal intensity while the area of the brain covered indicates spatial extent. Under neuromodulation conditions, both the signal intensity and the spatial extent is greater when compared to control conditions for each and all tongue directions **(Figure 3) (Figure SI-3).** Furthermore, the increased classification accuracy and area under the receiver-operator curve (AUC-ROC) indicate the increased consistency of the signal intensity. In particular, for all tongue movements concatenated versus baseline-tongue at rest, the neuromodulation condition's mean accuracy and AUC-ROC (94.3%, 0.997) were both significantly higher than the control condition's mean accuracy and AUC-ROC (89.6%, 0.985) ($p < 0.0001$). Similarly, for the up tongue direction and down tongue direction versus baseline-tongue at rest conditions, the mean accuracy and AUC-ROC were significantly higher for neuromodulation (Up: 95.9%, 0.959; Down: 96.5%, 0.964) compared to control conditions (Up: 90.0%, 0.991; Down: 90.8%, .995) ($p < 0.0001$).

A.

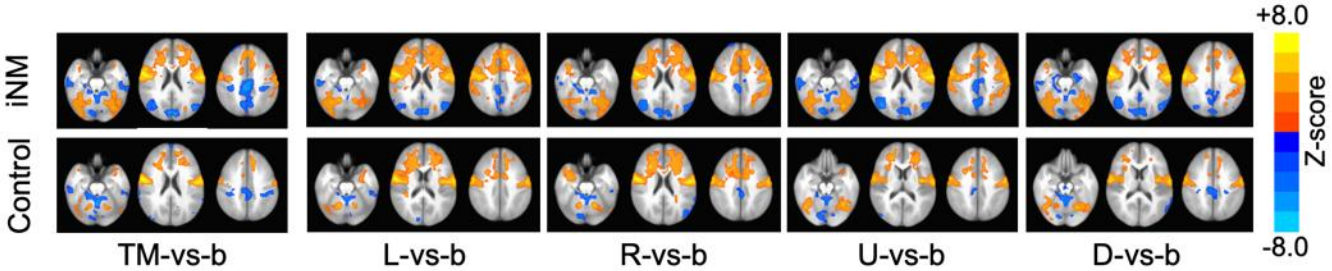

B.

Classification	Permutations	TM-vs-b	L-vs-b	R-vs-b	U-vs-b	D-vs-b
Accuracy	Train – Test: Control	89.6%	95.9%	96.0%	90.0%	90.8%
	Train – Test: iNM	94.3%	97.2%	97.7%	95.9%	96.5%
AUC	Train – Test: Control	.997	.994	.998	.991	.995
	Train – Test: iNM	.985	.989	.988	.959	.964

C.

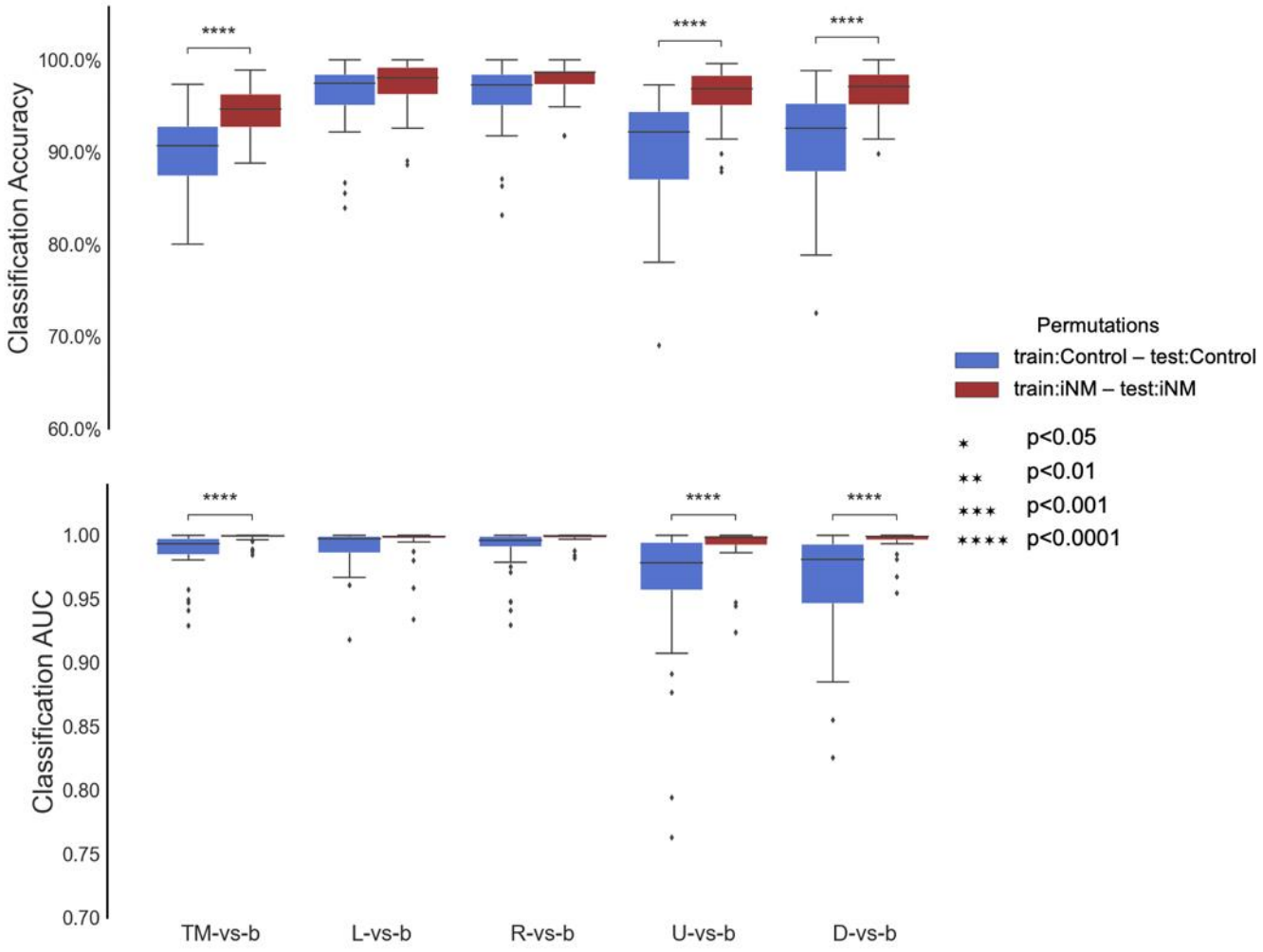

Figure 3. iNM increases consistency in the signal intensity and spatial extent compared to the control-no iNM condition using linear support vector machine analysis.

A. Decoding cortical networks that control selectivity for each tongue motor control direction. SVM-generated activation map for each tongue movement direction in iNM (top) and control – no iNM (bottom) conditions: voxelwise p value = 0.005, cluster size > 10 voxels
B. Table of SVM-generated classification accuracies and areas under the receiver-operator curve
C. Boxplot diagram of SVM-generated classification accuracies and areas under the receiver-operator curve (CA, y-axis) across all subjects as a function of different classifications (x-axis) and permutations of training-testing data types (color-coded). L=Left movement, R=Right movement, U=Up movement, D=Down movement, TM=Tongue Movement in all directions, b=Tongue Rest-baseline. On each box, the central line, the lower and upper edges represent the median (Q2), the 25th (Q1) and 75th (Q3) percentiles, respectively. The black open dots represent outliers (bigger than Q3 by 1.5*(Q3-Q1) or smaller than Q1 by 1.5*(Q3-Q1)). The whiskers extend to the most extreme non-outlier datapoints. The black lines and asterisks show significant differences as indicated by paired-samples Wilcoxon sign tests.

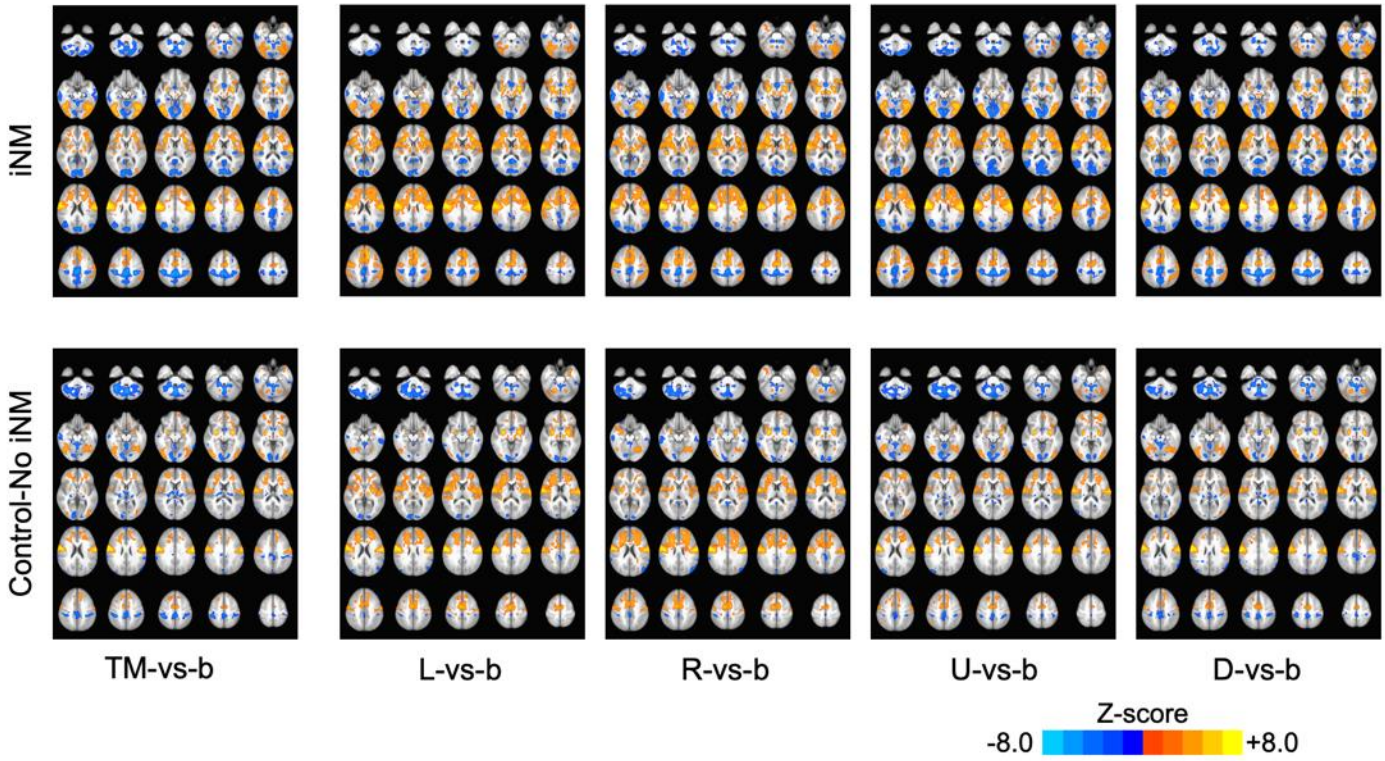

Figure SI-3. Cortical maps show that iNM increases consistency in the signal intensity and spatial extent compared to the control-no iNM condition using linear support vector machine analysis.
SVM-generated activation maps for each tongue motor control direction in iNM (top) and control – no iNM (bottom) conditions: voxelwise p value = 0.005, cluster size > 10 voxels

iNM (red) increases mean AUC signal intensity change compared to control-no iNM (blue) condition for each and across tongue motor control directions and networks.

The percent AUC signal intensity change illustrates the effect of neuromodulation on signal intensity over the course of each block within the run. In the motor network, there was an 8% increase in the AUC signal intensity change for all tongue directions concatenated versus baseline-tongue at rest. Similarly, the sensory network

displayed a 35% increase, the attention network a 36% increase, the reward network a 28% increase and all the networks concatenated a 26% increase in AUC signal intensity change. For the remaining individual tongue directions, the motor network displayed a range from 17%-24% increase, the sensory network a 41%-52% increase, the attention network a 28%-47% increase, the reward network a 6%-50% increase, and all the networks concatenated a 27%-39% increase in AUC signal intensity change. Overall, there was a increase in AUC signal intensities across each and all directions and networks that indicate neuromodulation does indeed increase the BOLD signal intensity. Furthermore, across each and all directions and networks, there was a range of 16% - 66% increase in the AUC signal intensity during the swallow period even when no neuromodulation was given during that block. When examining the baseline-tongue at rest period, a majority of the AUC signal intensity changes were positive ranging from 38% to 469% increase with the exception of the reward network during left tongue direction versus baseline-tongue at rest condition. Both these observations indicate that neuromodulation can have a carry-over effect even when no neuromodulation is given during the following blocks. **(Figure 4)** Detailed analysis's of each ROI for each direction can be found in the Supplemental Information. **(Figure SI-4, Figure SI-5, Figure SI-6)**

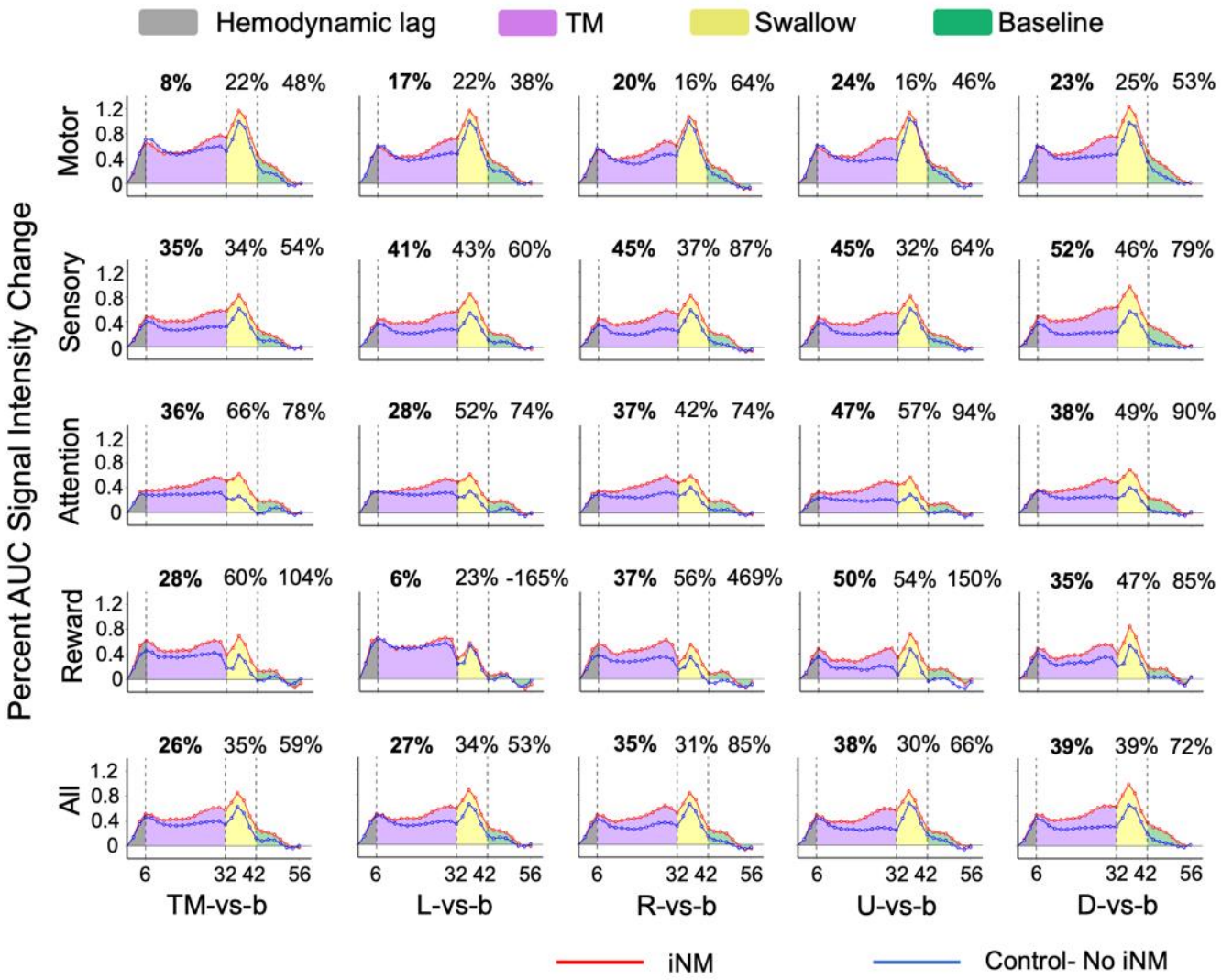

Figure 4. iNM (red) increases mean AUC signal intensity change compared to control-no iNM (blue) condition for each and across tongue motor control directions and networks, as a function of time: 1. cortical direction selectivity during tongue movement (6 – 32 seconds); 2. cortical selectivity during swallow (32 – 42 seconds); 3. cortical selectivity during baseline-tongue at rest (42 – 56 seconds). iNM effects transfer to swallow and baseline-tongue at rest blocks during which there is no neuromodulation applied.

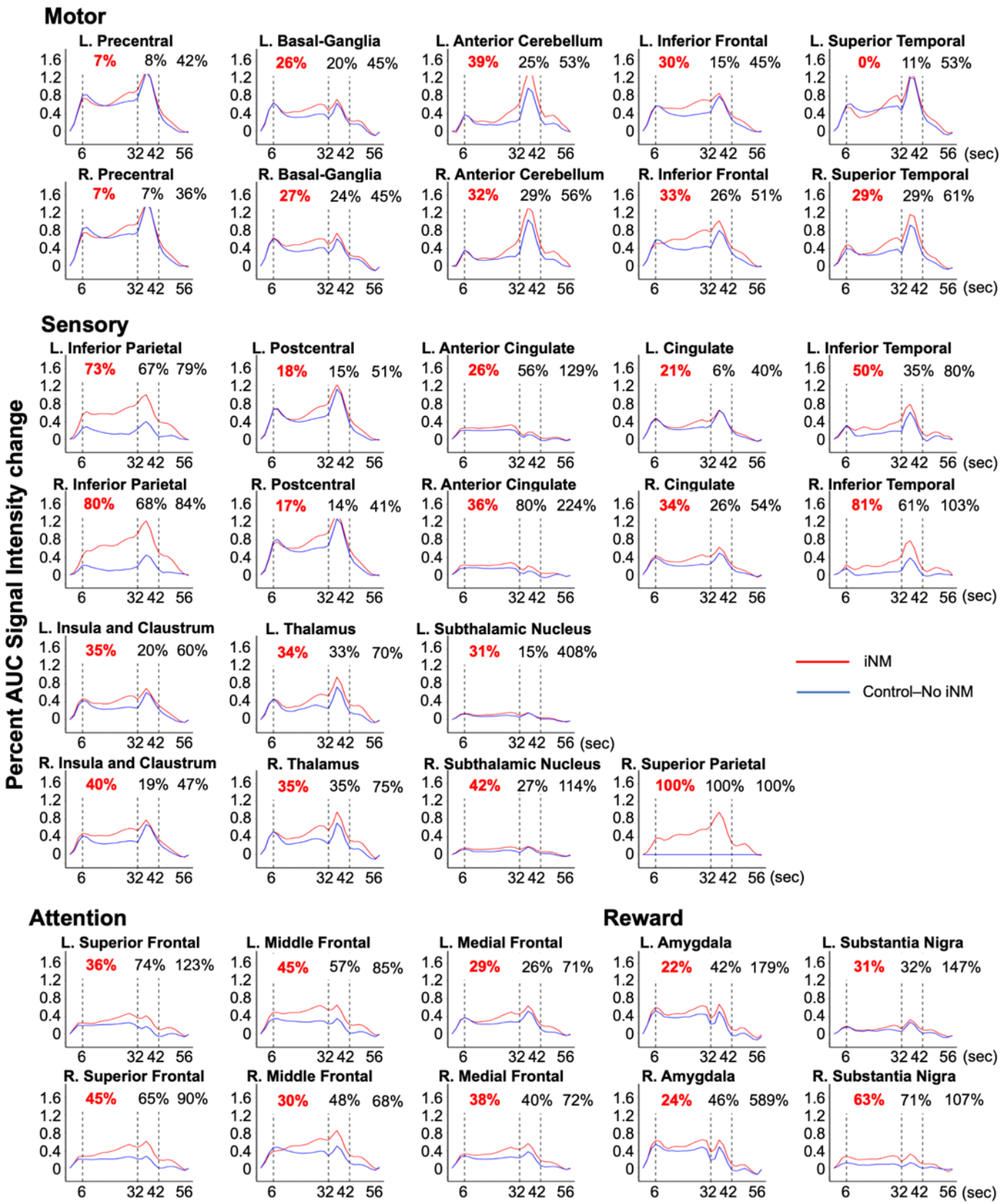

Figure SI-4. iNM (red) increases mean percent AUC signal intensity change compared to control-no iNM (blue) condition for each ROI within each network: 1. cortical direction selectivity during tongue movement (6 – 32 seconds); 2. cortical selectivity during swallow (32 – 42 seconds); 3. cortical selectivity during baseline-tongue at rest (42 – 56 seconds). iNM effects transfer to swallow and baseline-tongue at rest blocks during which there is no neuromodulation applied.

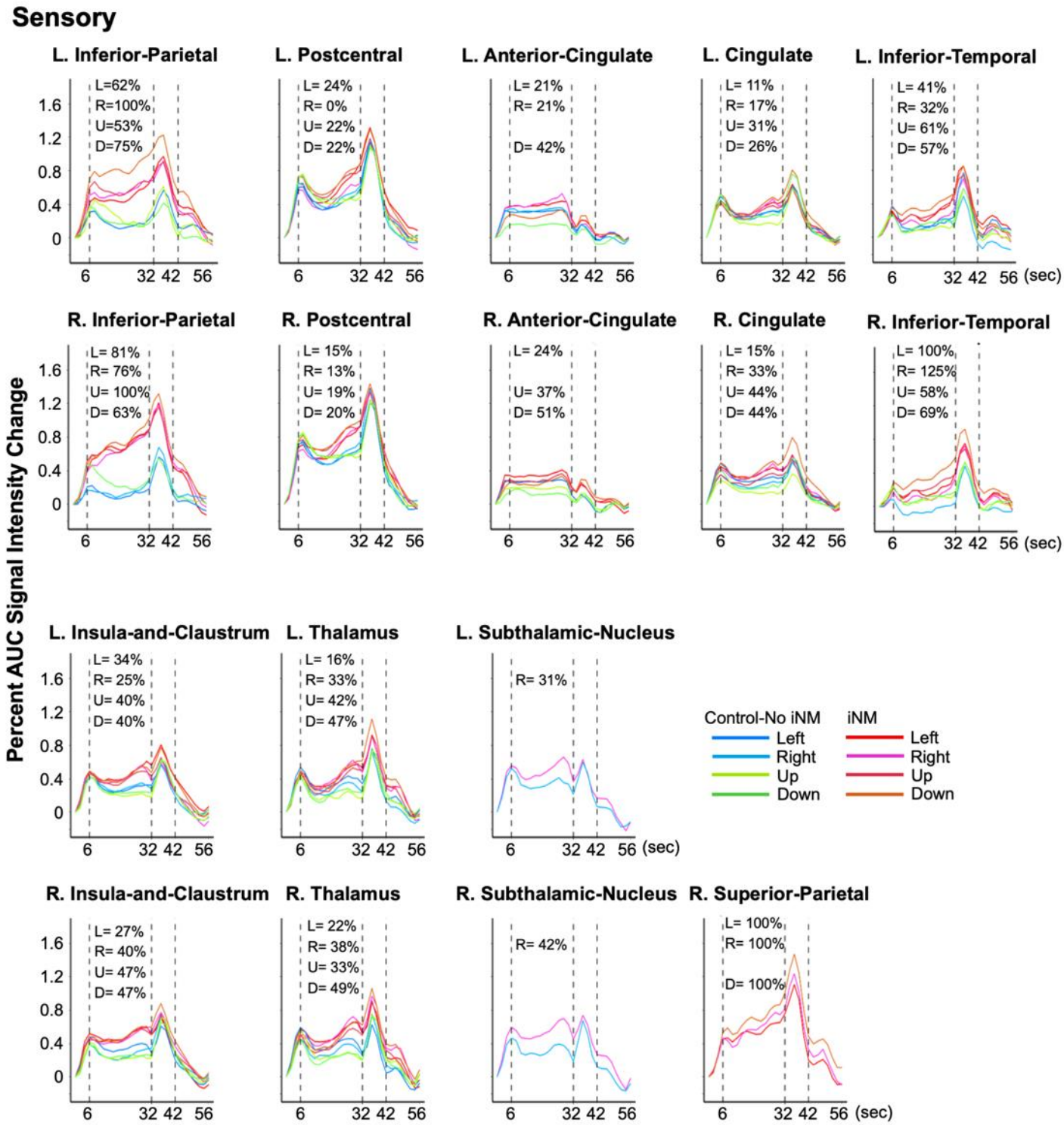

Figure SI-5. iNM increases mean percent AUC signal intensity change compared to control-no iNM condition for each cortical direction selectivity during tongue motor control (6 – 32 seconds) within each ROI that comprise the sensory network.

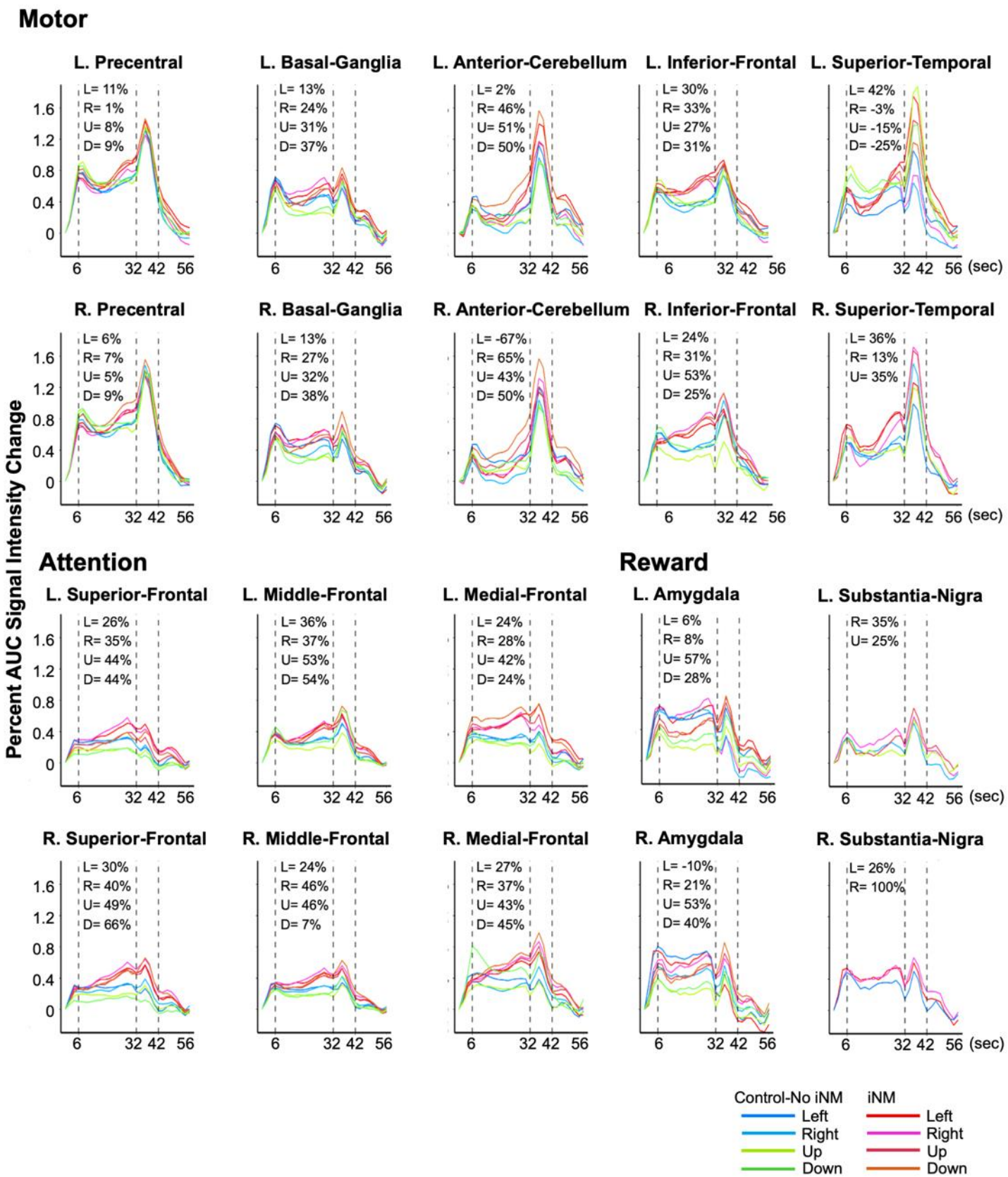

Figure SI-6. iNM increases mean percent AUC signal intensity change compared to control-no iNM condition for each cortical direction selectivity during tongue motor control (6 – 32 seconds) within each ROI that comprise the motor, attention, and reward networks.

iNM increases the sensitivity index (d') for each ROI within each network and across each and all tongue motor control directions compared to control-no iNM, as a function of time

The d' sensitivity index measures the separation between the means of the control and iNM distributions with respect to their standard deviations. For the motor network, the d' sensitivity index ranged from 60.4 to 62.9, while the AUC ranged from 10.9 to 27 for each and all tongue motor directions. Likewise, the sensory network's d' score ranged from 56.6 to 59.1, the attention network ranged from 57.6 to 61.1 and the reward network ranged from 58.8 to 68.2. The corresponding AUC's for the networks ranged from 41 to 50.1 for the sensory network, 27.8 to 45.9 for the attention network and 7.6 to 45.2 for the reward network. Overall, neuromodulation increased both the d' sensitivity index as well as the AUC for each network and across each and all tongue motor control directions. **(Figure 5)**

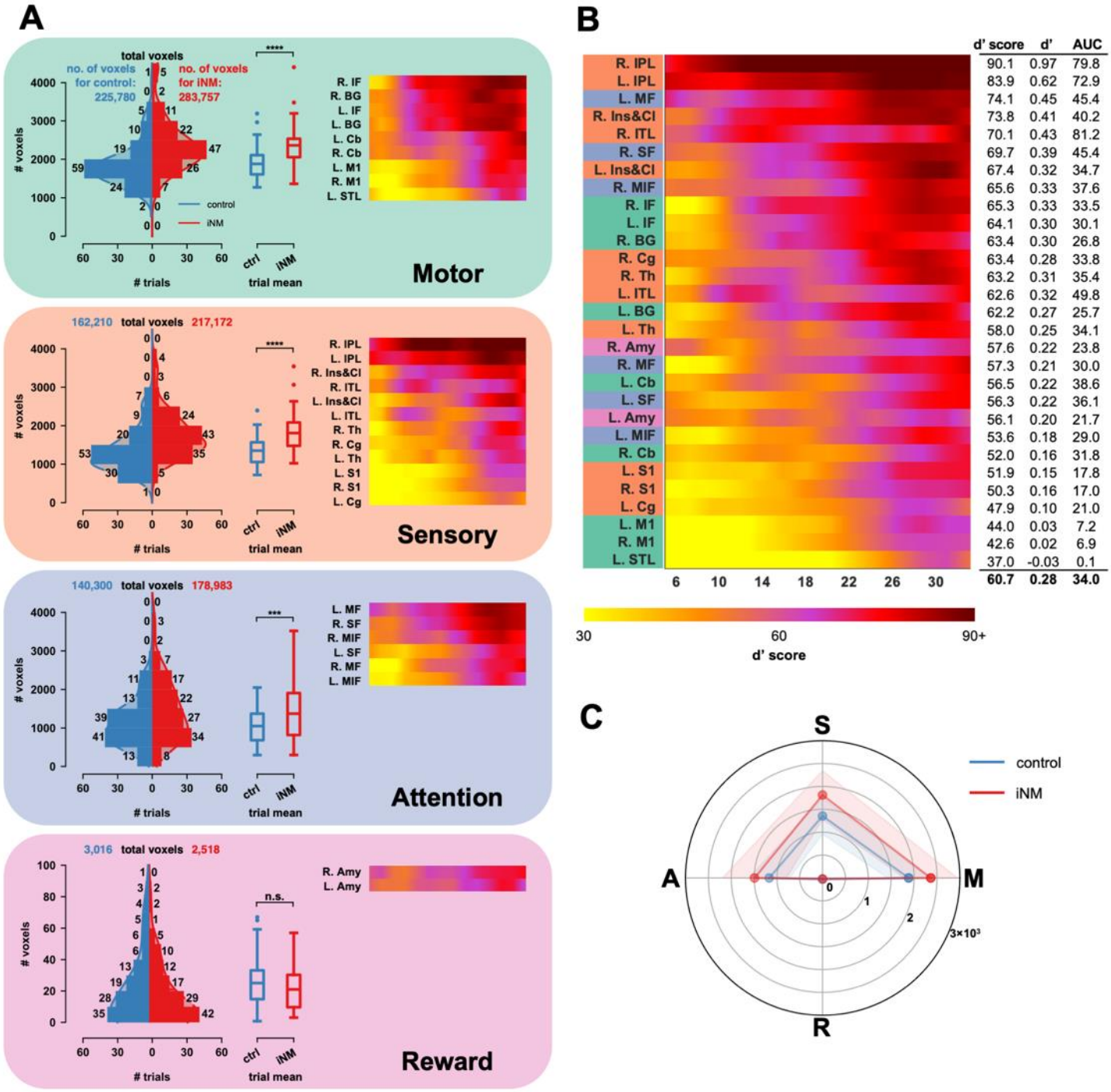

Figure 5. iNM increases the BOLD signal in both magnitude and spatial extent. (A) (*left*) For all ROIs within each network (motor, sensory, attention, or reward) under either control (blue) or iNM (red), the total number of voxels compromising the subset of ROIs for each trial (subject and direction) is shown in the histogram and kernel density estimate, and summarized in the adjacent box plots. (*right*) The means of the d'-generated scores and the percent BOLD signal AUC intensity change are presented in the heatmaps for each region, categorized by network. Color represents the mean d' score of the BOLD response between iNM and control conditions for a given time repetition across all trials. (**B**) The same heatmaps as in **A** are replicated in descending order of overall d' score across time. The ROI label colors correspond to networks color coded in **A**. The table displays mean d' score, d' value, and AUC for each region during the tongue movement interval (6-32 seconds). (**C**) The number of voxels per trial for all ROIs within a given network is shown for the motor (M), sensory (S), attention (A), and reward (R) networks. Solid lines and shaded areas indicate the mean and standard deviation, respectively, for the control (blue) and iNM (red) conditions.

iNM (red) overall decreases the mean percent AUC change of the BOLD intensity variance compared to the control-no iNM (blue) condition for most tongue motor control directions and networks

The percent AUC change of the BOLD signal intensity variance illustrates the effect of neuromodulation on BOLD signal variance over the course of each block within the run. In the motor network, there was an 9% decrease in the AUC change of the signal intensity variance for all tongue directions concatenated versus baseline-tongue at rest. Similarly, the sensory network displayed a 14% decrease, the attention network a 18% decrease, and all the networks concatenated a 11% decrease. The reward network; however, displayed a 2% increase. For the remaining individual tongue directions, the motor network displayed a range from 21% decrease to 7% increase, the sensory network from 22% decrease to 1% increase, the attention network a 25%-10% decrease, the reward network a 19% decrease to 12% increase, and all the networks concatenated a 20% decrease to a 2% increase. A majority of the AUC change of the BOLD signal intensity that increased occurred in the right tongue direction versus baseline-tongue at rest condition. However, overall, there was a decrease in AUC signal intensity variance for most directions and networks which indicates that neuromodulation does indeed decrease the variance of the BOLD signal intensity. Furthermore, across each and all directions and networks, there was a range of 36% to 3% decrease in the AUC signal intensity variance during the swallow period even when no neuromodulation was given during that block. When examining the baseline-tongue at rest period, there was a decrease in signal intensity variance ranging from 34% to 1% across each and all directions and networks. Both these observations indicate that neuromodulation can have a carry-over effect even when no neuromodulation is given during the following blocks. **(Figure 6).**

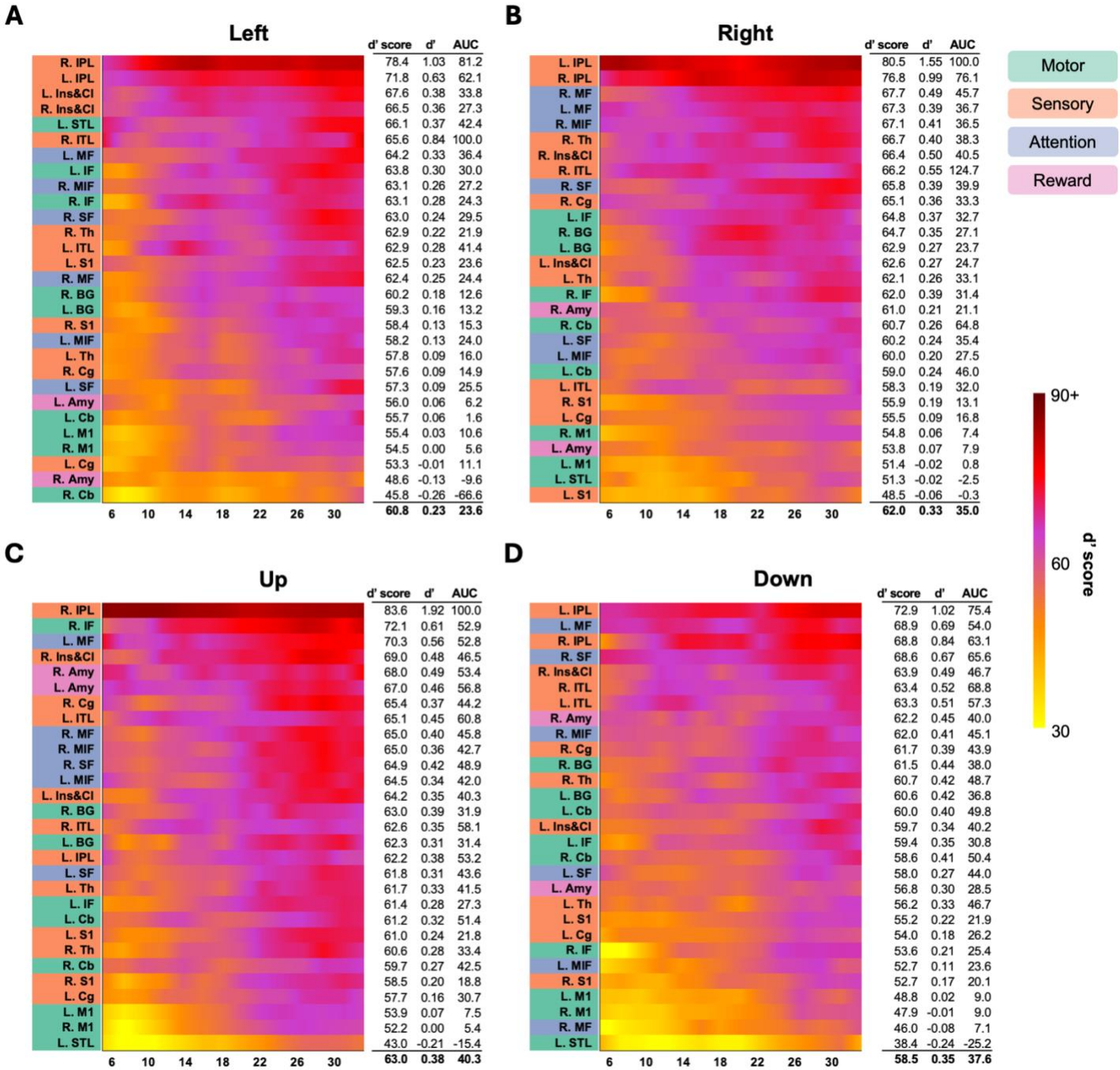

Figure SI-7: iNM increases the sensitivity index (d') for each ROI during individual tongue motor control directions compared to control, as a function of time. Similar to Figure 5, the heatmaps represent the mean d' score of each region that compares BOLD response between the iNM and control conditions, for a given time repetition. Tables display the mean d' score, d' value, and AUC during the tongue movement interval (6-32 seconds). Region labels are highlighted according to network. Data is shown for the left (**A**), right (**B**), up (**C**), and down (**D**) directions.

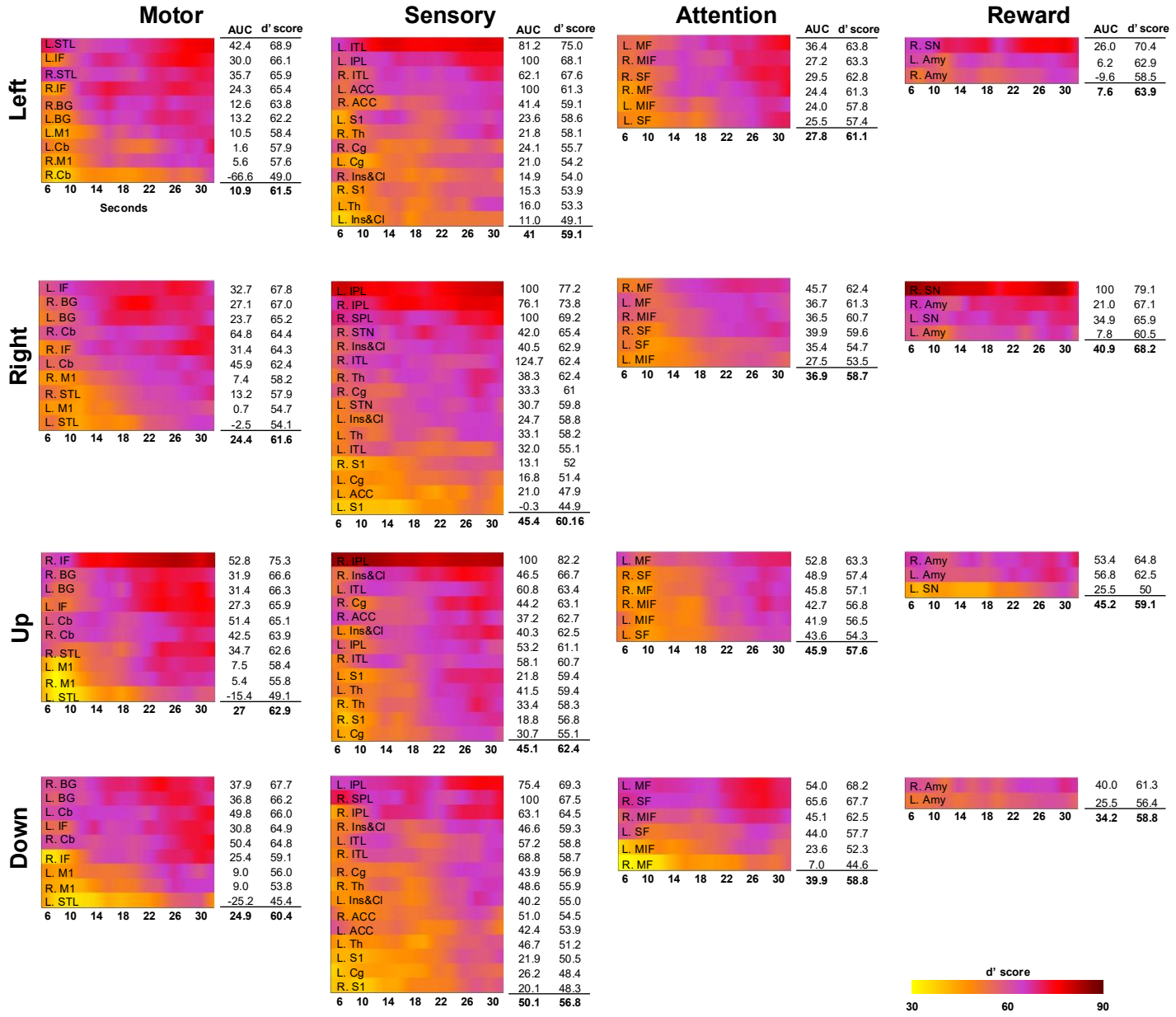

Figure SI-8: iNM increases the sensitivity index (d') for each ROI during individual tongue motor control directions compared to control, as a function of time. Heatmaps of the d' scores over time, as well as mean AUC and d' score per region, are shown as in Figure SI-7, except organized by both tongue movement direction and network.

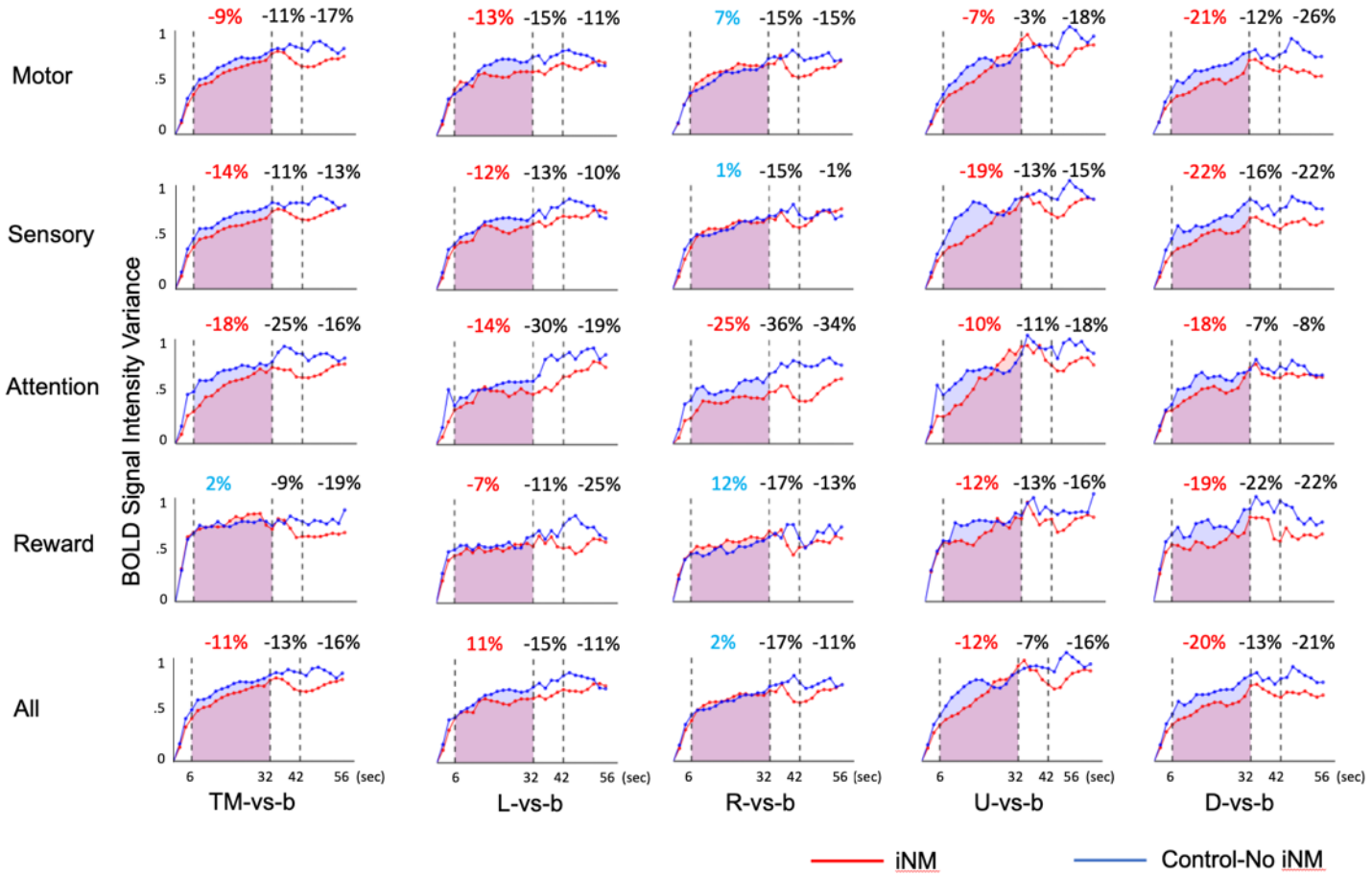

Figure 6. iNM (red) overall decreases the mean percent AUC change of the BOLD intensity variance compared to the control (blue) condition for most tongue motor control directions and networks, as a function of time: 1. cortical direction selectivity during tongue movement (6 – 32 seconds) 2. cortical selectivity during swallow (32 – 42 seconds) 3. cortical selectivity during baseline-tongue at rest (42 – 56 seconds). Negative (positive) values correspond to iNM-induced decreases (increases) of variance. iNM effects transfer to swallow and baseline-tongue at rest blocks during which there is no neuromodulation applied.

iNM increases Motor(M)-to-Motor(M), M-to-Sensory (S), M-to-Attention(A), S-to-S, S-to-M, S-to-A, A-to-A, A-to-M, and A-to-S network connectivities across all tongue motor control directions elucidated via dynamic causal modeling: Autoregressive Hidden Markov Model (AHMM).

The AHMM model identified two dynamic network states: state one associated with tongue motor and sensory control and state 2 associated with swallow. During neuromodulation, state 1 was upregulated in the tongue motor control block (95% vs 76%), the swallow block (78% vs 45%) and the baseline block (96% vs 75%). Furthermore, neuromodulation downregulated state 2 across all blocks as well, indicating that iNM enhances TMSC activation while significantly reducing interference from the swallow state. AHMM also computed connectivities between ROI's within each network for state 1 and illustrated that neuromodulation increases Motor(M)-to-Motor(M), M-to-Sensory (S), M-to-Attention(A), S-to-S, S-to-M, S-to-A, A-to-A, A-to-M, and A-to-S network connectivities across all tongue motor control directions concatenated. Furthermore, significance testing illustrated specific ROI connectivities that were either upregulated or downregulated as a result of neuromodulation. **(Figure 7)** More detailed information regarding the connectivities and dynamic state models across each tongue direction can be found in the Supplemental Information **(Figure SI-7).**

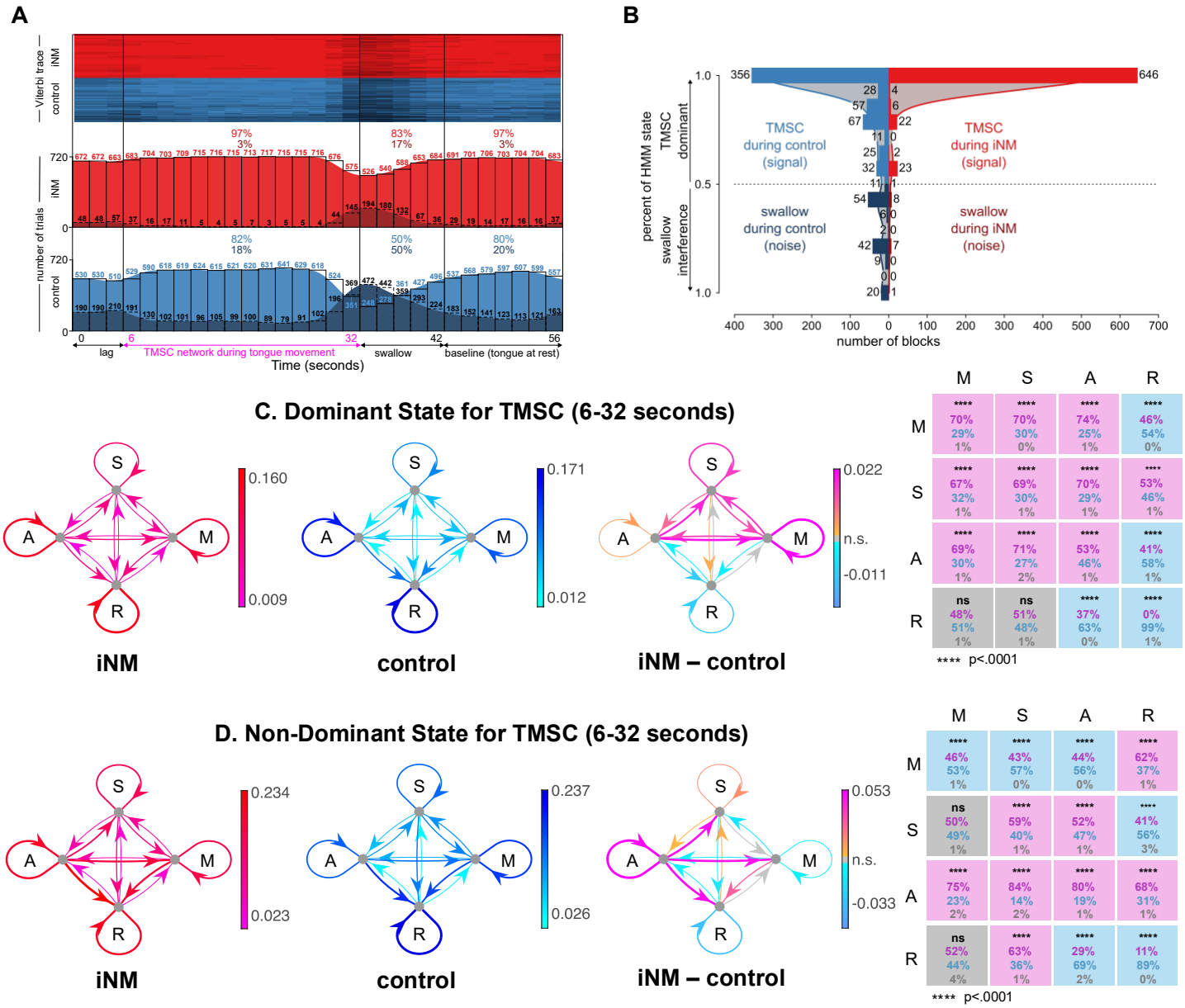

Figure 7. iNM increases Motor(M)-to-Motor(M), M-to-Sensory(S), M-to-Attention(A), S-to-S, S-to-M, S-to-A, A-to-A, A-to-M, and A-to-S network connectivities across all tongue motor control directions elucidated via dynamic causal modeling: Autoregressive Hidden Markov Model (AHMM).

A. We selected the timeseries from the brain areas that select for tongue movement. Our autoregressive hidden Markov model (aHMM) was fit to the brain areas that selected for tongue movement (6-32 seconds). Model inference was then performed on the entire timeseries (0-56 seconds). (top) Viterbi trace for iNM (red) and control (blue) trials that characterize each brain state during TM, swallow, and baseline intervals for each condition. (bottom) Histogram of the number of trials corresponding to TMSC (light red/blue) or swallow (dark red/blue) brain state for each time repetition, divided into the iNM (red) and control (blue) conditions. Percentages correspond to the fraction of trials within each brain state across the TM, swallow, or baseline intervals. **B.** The histogram compares the signal (TMSC state, red/blue) and noise (swallow state, dark red/dark blue) by displaying the number of trials in each bin that correspond to each of the two states (total trials (iNM vs. control): 727 vs. 525 (TMSC state), 15 vs. 195 (swallow state)). Shaded curves represent the kernel density estimate (KDE) fit to the binned data for the iNM and control conditions. The KDE was calculated by the summation of normal distributions centered at each data point, followed by normalization, to generate a smoothed estimate of the histogram bins. KDE bandwidth was estimated via Scott's method, and boundary corrections at 0 and 1 employed reflection of the data across the boundaries. **C-D.** For the dominant (TMSC) or non-dominant state, the strength

of ROI-to-ROI connections within networks (M = Motor network, S = Sensory network, A = Attention network, R = Reward network) is quantified as the mean absolute value of the autoregressive coefficients during the iNM (fuchsia/red) or control (light/dark blue) condition, or the difference in absolute values between conditions (orange/fuchsia and light/dark blue indicate increased/decreased during iNM, respectively). At far right, significant increases (fuchsia), decreases (light blue), or insignificant differences (gray) in these network-to-network connectivities are shown for iNM compared to control. Percentages indicate the fraction of region-to-region connectivities within each network-to-network connection that are increased (fuchsia), decreased (light blue), or insignificant (gray) in iNM compared to control. Correction for multiple comparisons used an FDR of 0.05.

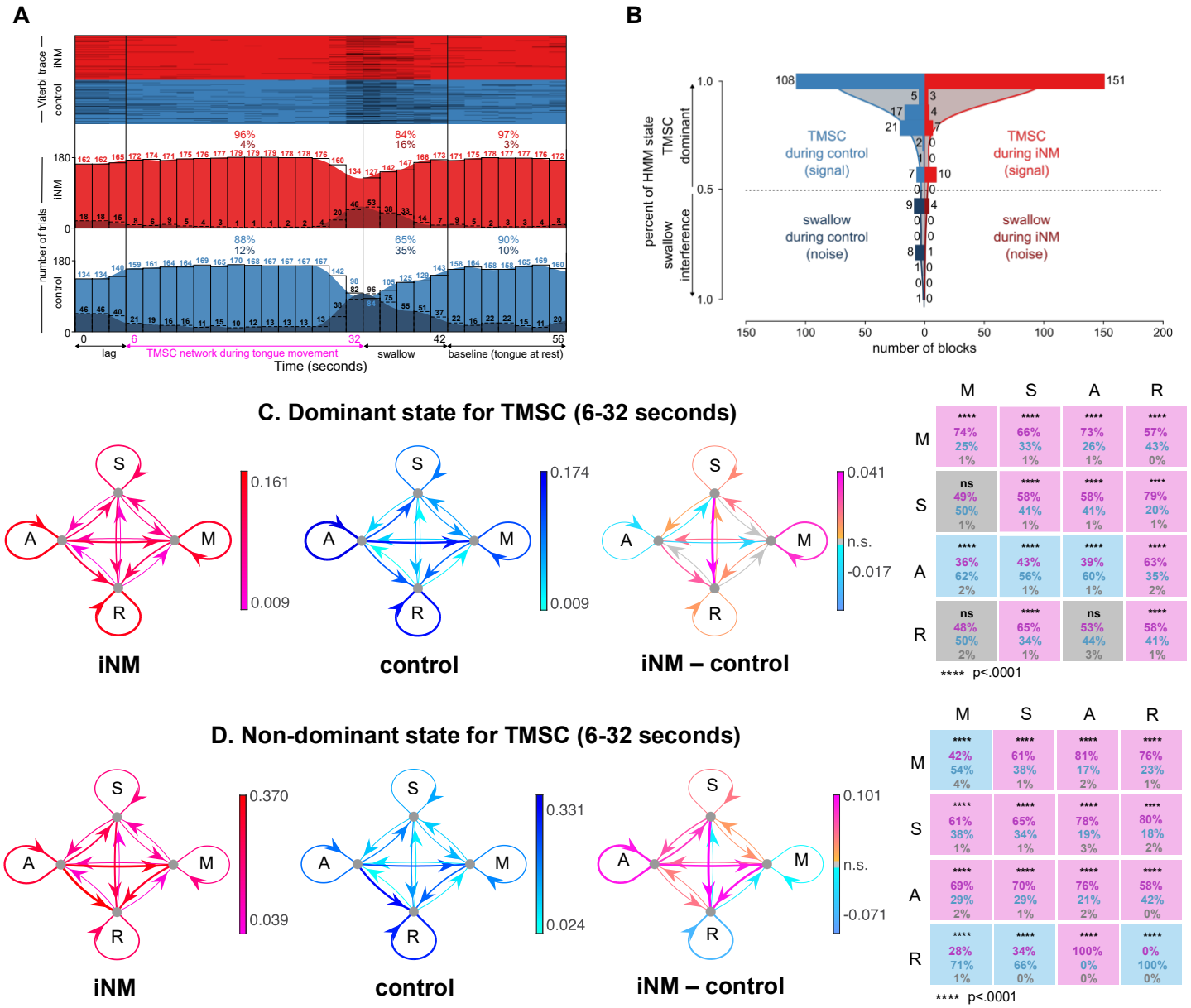

Figure SI-9: Autoregressive Hidden Markov Model (aHMM) for trials corresponding to the left tongue movement direction. Panels (**A-D**) as per caption for Figure 7.

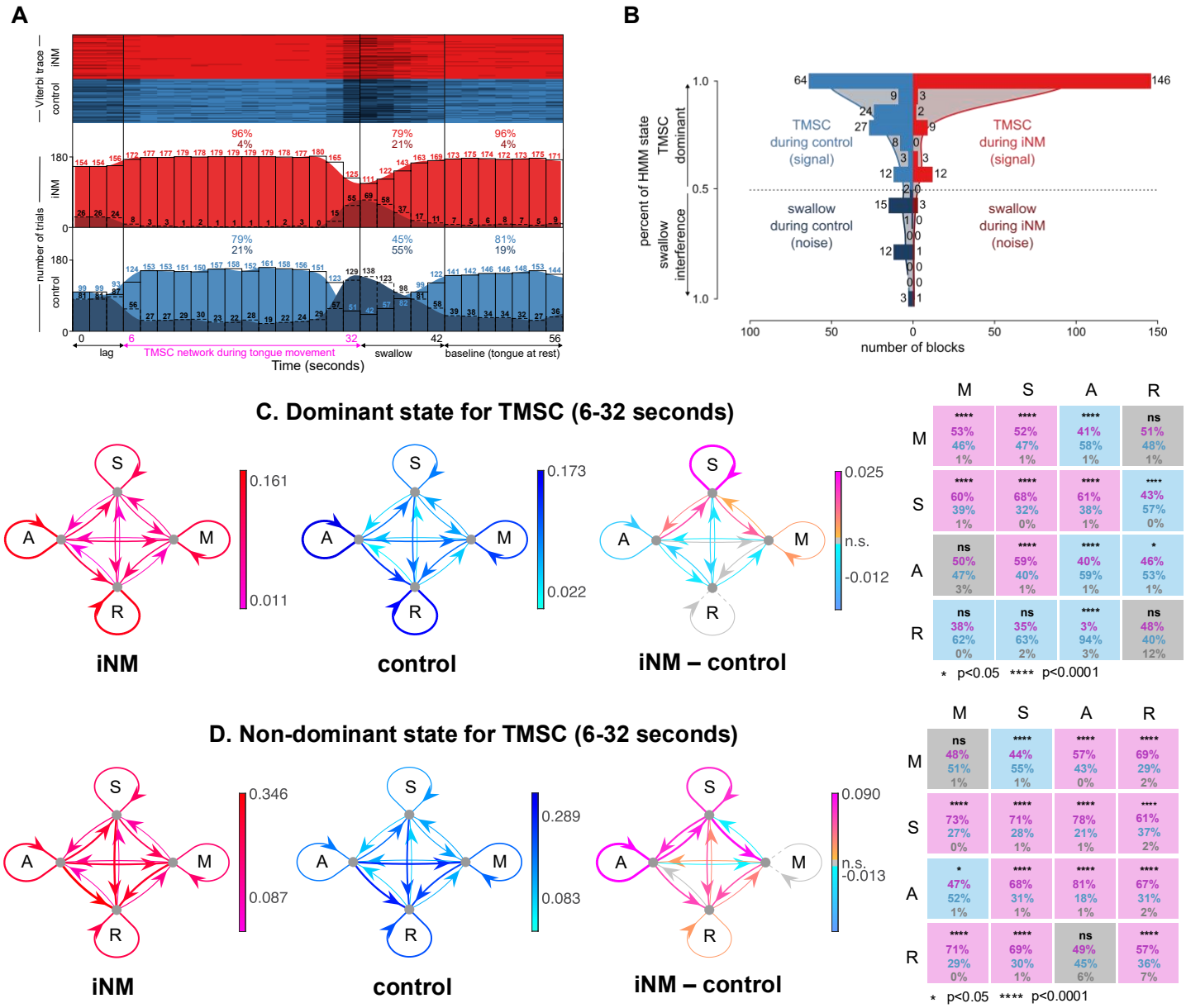

Figure SI-10: Autoregressive Hidden Markov Model (aHMM) for trials corresponding to the right tongue movement direction. Panels (**A-D**) as per caption for Figure 7.

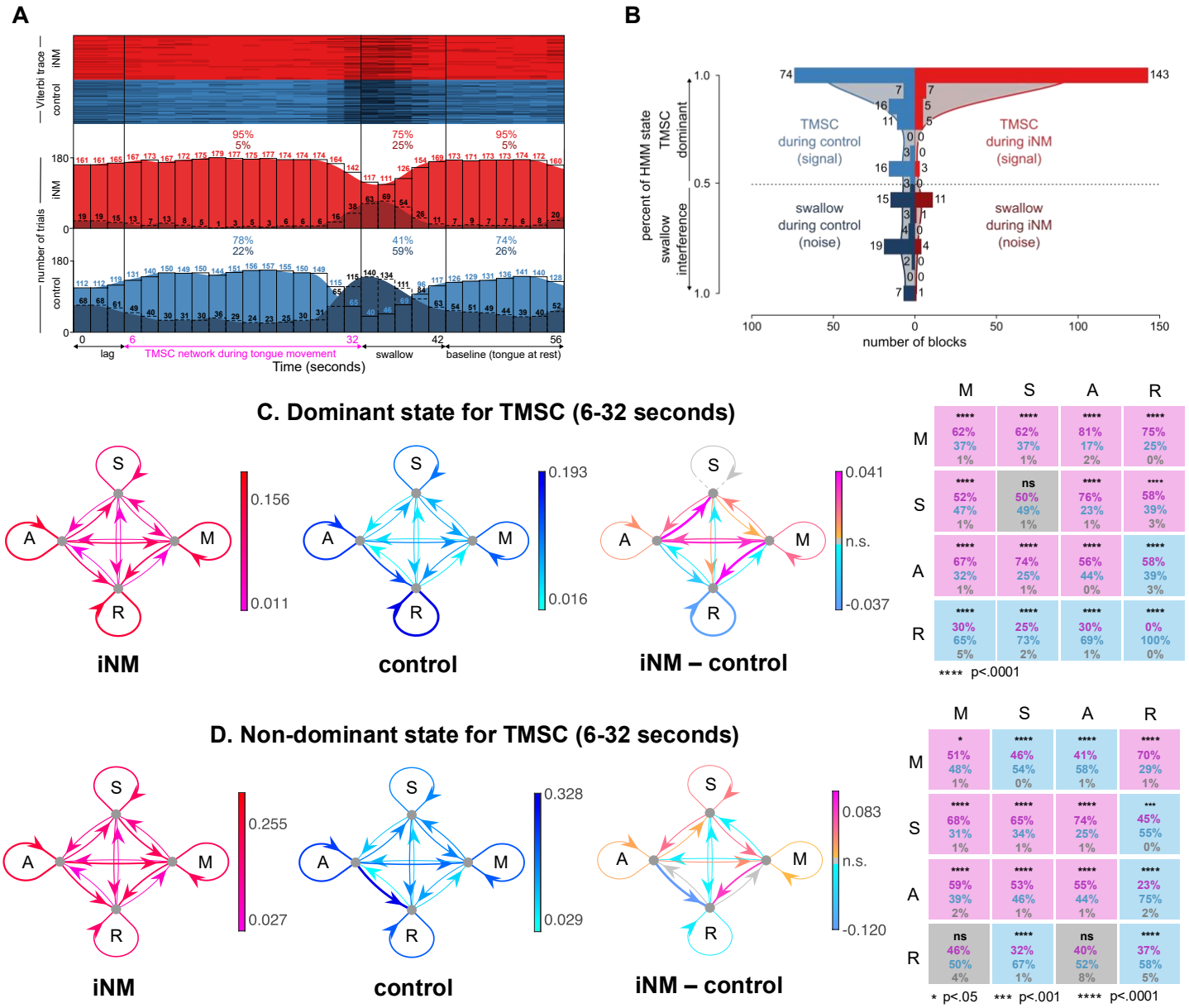

Figure SI-11: Autoregressive Hidden Markov Model (aHMM) for trials corresponding to the up tongue movement direction. Panels (**A-D**) as per caption for Figure 7.

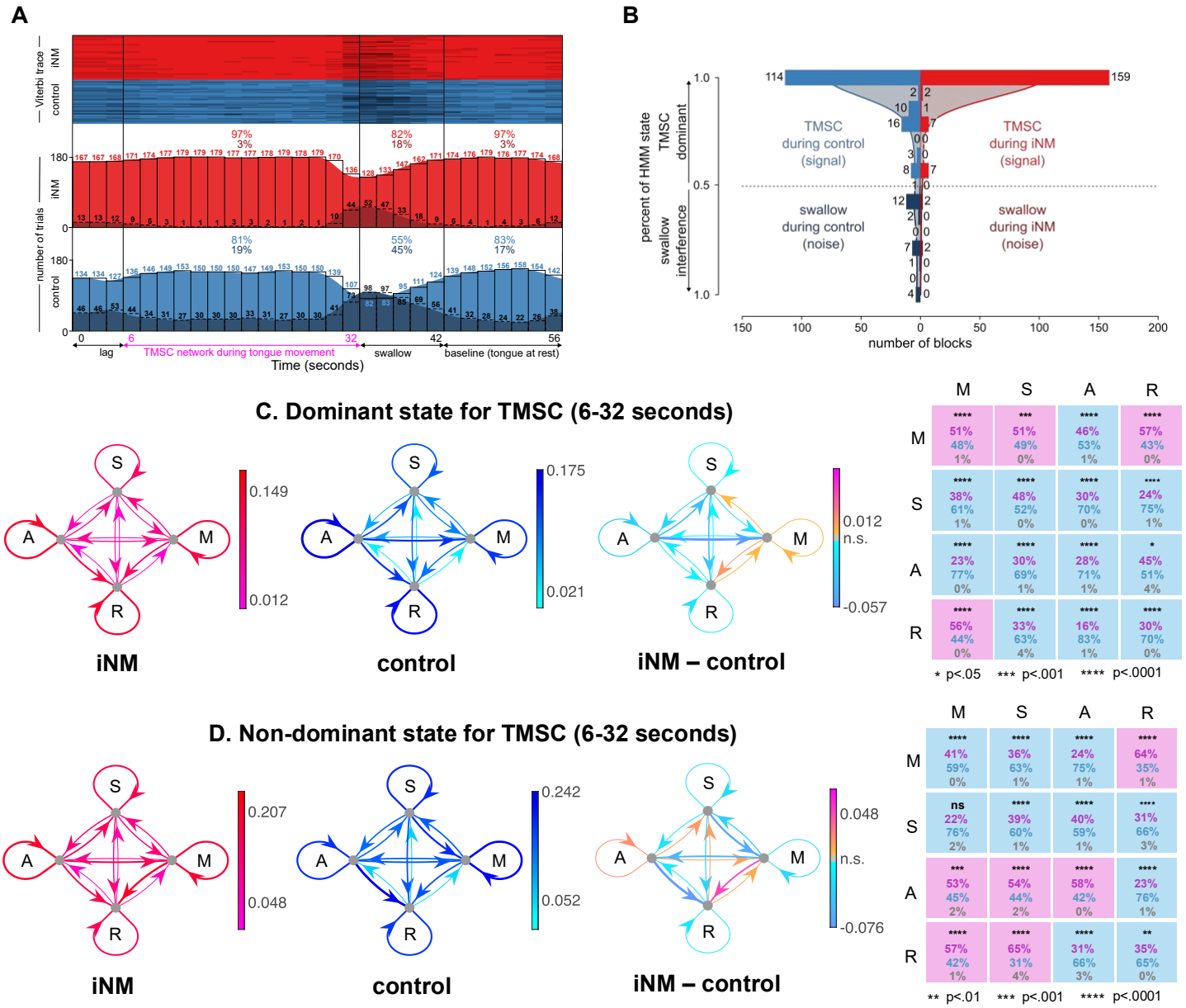

Figure SI-12: Autoregressive Hidden Markov Model (aHMM) for trials corresponding to the down tongue movement direction. Panels (**A-D**) as per caption for Figure 7.

References

1. O'Connell NE, Marston L, Spencer S, DeSouza LH, Wand BM. Non-invasive brain stimulation techniques for chronic pain. *Cochrane Database of Systematic Reviews*. Published online March 16, 2018. doi:10.1002/14651858.CD008208.pub4
2. Yang S, Chang MC. Effect of Repetitive Transcranial Magnetic Stimulation on Pain Management: A Systematic Narrative Review. *Front Neurol*. 2020;11. doi:10.3389/fneur.2020.00114
3. Alwardat M, Pisani A, Etoom M, et al. Is transcranial direct current stimulation (tDCS) effective for chronic low back pain? A systematic review and meta-analysis. *J Neural Transm*. 2020;127(9):1257-1270. doi:10.1007/s00702-020-02223-w
4. Gibson W, Wand BM, O'Connell NE. Transcutaneous electrical nerve stimulation (TENS) for neuropathic pain in adults. *Cochrane Database of Systematic Reviews*. 2017;2021(3). doi:10.1002/14651858.CD011976.pub2
5. Siddall PJ, Cousins MJ. Persistent Pain as a Disease Entity: Implications for Clinical Management. *Anesth Analg*. Published online August 2004:510-520. doi:10.1213/01.ANE.0000133383.17666.3A
6. Woolf CJ. Somatic pain–pathogenesis and prevention. *Br J Anaesth*. 1995;75(2):169-176. doi:10.1093/bja/75.2.169
7. Craig AD. How do you feel? Interoception: the sense of the physiological condition of the body. *Nat Rev Neurosci*. 2002;3(8):655-666. doi:10.1038/nrn894
8. Cameron OG. *Visceral Sensory Neuroscience: Interoception*.; 2001.
9. Garfinkel SN, Critchley HD. Interoception, emotion and brain: new insights link internal physiology to social behaviour. Commentary on: *Soc Cogn Affect Neurosci*. 2013;8(3):231-234. doi:10.1093/scan/nss140
10. Nicholas M, Vlaeyen JWS, Rief W, et al. The IASP classification of chronic pain for ICD-11: chronic primary pain. *Pain*. 2019;160(1):28-37. doi:10.1097/j.pain.0000000000001390
11. Craig AD (Bud). The sentient self. *Brain Struct Funct*. 2010;214(5-6):563-577. doi:10.1007/s00429-010-0248-y
12. (Bud) Craig A. Interoception: the sense of the physiological condition of the body. *Curr Opin Neurobiol*. 2003;13(4):500-505. doi:10.1016/S0959-4388(03)00090-4
13. Lowell SY, Reynolds RC, Chen G, Horwitz B, Ludlow CL. Functional connectivity and laterality of the motor and sensory components in the volitional swallowing network. *Exp Brain Res*. 2012;219(1):85-96. doi:10.1007/s00221-012-3069-9
14. Di Lernia D, Lacerenza M, Ainley V, Riva G. Altered Interoceptive Perception and the Effects of Interoceptive Analgesia in Musculoskeletal, Primary, and Neuropathic Chronic Pain Conditions. *J Pers Med*. 2020;10(4):201. doi:10.3390/jpm10040201
15. Hutcheson KA, Yuk M, Hubbard R, et al. Delayed lower cranial neuropathy after oropharyngeal intensity-modulated radiotherapy: A cohort analysis and literature review. *Head Neck*. 2017;39(8):1516-1523. doi:10.1002/hed.24789
16. Dong Y, Ridge JA, Ebersole B, et al. Incidence and outcomes of radiation-induced late cranial neuropathy in 10-year survivors of head and neck cancer. *Oral Oncol*. 2019;95:59-64. doi:10.1016/j.oraloncology.2019.05.014
17. JANSSEN S, GLANZMANN C, YOUSEFI B, et al. Radiation-induced lower cranial nerve palsy in patients with head and neck carcinoma. *Mol Clin Oncol*. 2015;3(4):811-816. doi:10.3892/mco.2015.558
18. Lin Y, Jen Y, Lin J. Radiation-related cranial nerve palsy in patients with nasopharyngeal carcinoma. *Cancer*. 2002;95(2):404-409. doi:10.1002/cncr.10668
19. Kong L, Lu JJ, Liss AL, et al. Radiation-Induced Cranial Nerve Palsy: A Cross-Sectional Study of Nasopharyngeal Cancer Patients After Definitive Radiotherapy. *International Journal of Radiation Oncology*Biology*Physics*. 2011;79(5):1421-1427. doi:10.1016/j.ijrobp.2010.01.002
20. Awan MJ, Mohamed ASR, Lewin JS, et al. Late radiation-associated dysphagia (late-RAD) with lower cranial neuropathy after oropharyngeal radiotherapy: A preliminary dosimetric comparison. *Oral Oncol*. 2014;50(8):746-752. doi:10.1016/j.oraloncology.2014.05.003

21. Buttermann GR. Anterior cervical discectomy and fusion outcomes over 10 years: A prospective study. *Spine (Phila Pa 1976)*. 2018;43(3):207-214. doi:10.1097/BRS.0000000000002273
22. Zhang Y, Yang G, Zhou T, et al. Efficacy and safety of anterior cervical discectomy and fusion (ACDF) through mini-incision and posterior laminoplasty (LAMP) for treatment of long-level cervical spondylosis: a retrospective cohort study. *BMC Surg*. 2022;22(1):115. doi:10.1186/S12893-022-01567-2
23. Saifi C, Fein AW, Cazzulino A, et al. Trends in resource utilization and rate of cervical disc arthroplasty and anterior cervical discectomy and fusion throughout the United States from 2006 to 2013. *Spine Journal*. 2018;18(6):1022-1029. doi:10.1016/j.spinee.2017.10.072
24. Marquez-Lara A, Nandyala S V., Fineberg SJ, Singh K. Current trends in demographics, practice, and in-hospital outcomes in cervical spine surgery: A national database analysis between 2002 and 2011. *Spine (Phila Pa 1976)*. 2014;39(6):476-481. doi:10.1097/BRS.0000000000000165
25. An SB, Lee JJ, Kim TW, et al. Upper Cervical Surgery, Increased Signal Intensity of the Spinal Cord, and Hypertension as Risk Factors for Dyspnea after Multilevel Anterior Cervical Discectomy and Fusion. *Spine (Phila Pa 1976)*. 2020;45(7):E379-E386. doi:10.1097/BRS.0000000000003329
26. Murata S, Iwasaki H, Oka H, et al. A novel technique using ultrasonography in upper airway management after anterior cervical decompression and fusion. *BMC Med Imaging*. 2022;22(1). doi:10.1186/S12880-022-00792-8
27. Schroeder J, Weinstein J, Salzmann SN, et al. Effect of Steroid-Soaked Gelatin Sponge on Soft Tissue Swelling Following Anterior Cervical Discectomy and Fusion: A Radiographic Analysis. *Asian Spine J*. 2018;12(4):656. doi:10.31616/ASJ.2018.12.4.656
28. Maza NM, Ferrer CE, Qureshi SA, Cho SK, Chaudhary SB, Hecht AC. Contained-Delivery Route and the Administration of Postoperative Steroids Following Anterior Cervical Spinal Fusion with Low-dose rhBMP-2 Reduces the Magnitude of Respiratory Compromise. *Clin Spine Surg*. 2019;32(10):E420-E425. doi:10.1097/BSD.0000000000000850
29. Alsoof D, Perry J, Yang DS, et al. Risk of Dysphagia and Dysphonia in Patients With Prior Thyroidectomy Undergoing Anterior Cervical Discectomy and Fusion. *https://doi.org/101177/21925682221111095*. Published online July 14, 2022. doi:10.1177/21925682221111095
30. Latka D, Kozlowska K, Miekisiak G, et al. Safety and efficacy of cervical disc arthroplasty in preventing the adjacent segment disease: a meta-analysis of mid- to long-term outcomes in prospective, randomized, controlled multicenter studies. *Ther Clin Risk Manag*. 2019;15:531. doi:10.2147/TCRM.S196349
31. Winslow CP, Winslow TJ, Wax MK. Dysphonia and Dysphagia Following the Anterior Approach to the Cervical Spine. *Arch Otolaryngol Head Neck Surg*. 2001;127(1):51-55. doi:10.1001/ARCHOTOL.127.1.51
32. Baron EM, Soliman AMS, Simpson L, Gaughan JP, Young WF. Dysphagia, Hoarseness, and Unilateral True Vocal Fold Motion Impairment following Anterior Cervical Diskectomy and Fusion. *https://doi.org/101177/000348940311201102*. 2003;112(11):921-926. doi:10.1177/000348940311201102
33. Saifi C, Fein AW, Cazzulino A, et al. Trends in resource utilization and rate of cervical disc arthroplasty and anterior cervical discectomy and fusion throughout the United States from 2006 to 2013. *The Spine Journal*. 2018;18(6):1022-1029. doi:10.1016/j.spinee.2017.10.072
34. Marquez-Lara A, Nandyala S V., Fineberg SJ, Singh K. Current Trends in Demographics, Practice, and In-Hospital Outcomes in Cervical Spine Surgery. *Spine (Phila Pa 1976)*. 2014;39(6):476-481. doi:10.1097/BRS.0000000000000165
35. Epstein NE. A Review of Complication Rates for Anterior Cervical Diskectomy and Fusion (ACDF). *Surg Neurol Int*. 2019;10(100). doi:10.25259/SNI-191-2019
36. Fountas KN, Kapsalaki EZ, Nikolakakos LG, et al. Anterior cervical discectomy and fusion associated complications. *Spine (Phila Pa 1976)*. 2007;32(21):2310-2317. doi:10.1097/BRS.0B013E318154C57E
37. Nachalon Y. Anterior cervical spine surgery and dysphagia. *Curr Opin Otolaryngol Head Neck Surg*. 2022;30(6):417-421. doi:10.1097/MOO.0000000000000845
38. Frempong-Boadu A, Houten JK, Osborn B, et al. Swallowing and speech dysfunction in patients undergoing anterior cervical discectomy and fusion: a prospective, objective preoperative and

postoperative assessment. *J Spinal Disord Tech*. 2002;15(5):362-368. doi:10.1097/00024720-200210000-00004
39. Vaishnav AS, Saville P, McAnany S, et al. Predictive Factors of Postoperative Dysphagia in Single-Level Anterior Cervical Discectomy and Fusion. *Spine (Phila Pa 1976)*. 2019;44(7):E400-E407. doi:10.1097/BRS.0000000000002865
40. Tasiou A, Giannis T, Brotis AG, et al. Anterior cervical spine surgery-associated complications in a retrospective case-control study. *Journal of Spine Surgery*. 2017;3(3):444. doi:10.21037/JSS.2017.08.03
41. Kalb S, Reis MT, Cowperthwaite MC, et al. Dysphagia After Anterior Cervical Spine Surgery: Incidence and Risk Factors. *World Neurosurg*. 2012;77(1):183-187. doi:10.1016/J.WNEU.2011.07.004
42. Riley LH, Vaccaro AR, Dettori JR, Hashimoto R. Postoperative dysphagia in anterior cervical spine surgery. *Spine (Phila Pa 1976)*. 2010;35(SUPPL. 9S). doi:10.1097/BRS.0B013E3181D81A96
43. Alentado VJ, Bisson EF, Potts EA. Dysphagia after cervical spine surgery: a review of risk factors and preventative measures. *J Neurosurg Spine*. 2022;38(3):382-388. doi:10.3171/2022.11.SPINE221247
44. Liu FY, Yang DL, Huang WZ, et al. Risk factors for dysphagia after anterior cervical spine surgery: A meta-analysis. *Medicine*. 2017;96(10). doi:10.1097/MD.0000000000006267
45. Liu JM, Tong WL, Chen XY, et al. The incidences and risk factors related to early dysphagia after anterior cervical spine surgery: A prospective study. *PLoS One*. 2017;12(3). doi:10.1371/JOURNAL.PONE.0173364
46. Perez-Roman RJ, Luther EM, McCarthy D, et al. National Trends and Correlates of Dysphagia After Anterior Cervical Discectomy and Fusion Surgery. *Neurospine*. 2021;18(1):147. doi:10.14245/NS.2040452.226
47. Fehlings MG, Smith JS, Kopjar B, et al. Perioperative and delayed complications associated with the surgical treatment of cervical spondylotic myelopathy based on 302 patients from the AOSpine North America Cervical Spondylotic Myelopathy Study: Presented at the 2011 Spine Section Meeting. *J Neurosurg Spine*. 2012;16(5):425-432. doi:10.3171/2012.1.SPINE11467
48. Joseph JR, Smith BW, Mummaneni P V., La Marca F, Park P. Postoperative dysphagia correlates with increased morbidity, mortality, and costs in anterior cervical fusion. *Journal of Clinical Neuroscience*. 2016;31:172-175. doi:10.1016/j.jocn.2016.03.011
49. Song KJ, Lee SK, Ko JH, Yoo MJ, Kim DY, Lee KB. The clinical efficacy of short-term steroid treatment in multilevel anterior cervical arthrodesis. *The Spine Journal*. 2014;14(12):2954-2958. doi:10.1016/J.SPINEE.2014.06.005
50. Lee SH, Kim KT, Suk KS, Park KJ, Oh K Il. Effect of retropharyngeal steroid on prevertebral soft tissue swelling following anterior cervical discectomy and fusion: A prospective, randomized study. *Spine (Phila Pa 1976)*. 2011;36(26):2286-2292. doi:10.1097/BRS.0B013E318237E5D0
51. Yerneni K, Burke JF, Nichols N, Tan LA. Delayed Recurrent Laryngeal Nerve Palsy Following Anterior Cervical Discectomy and Fusion. *World Neurosurg*. 2019;122:380-383. doi:10.1016/J.WNEU.2018.11.066
52. Song J, Yi P, Wang Y, et al. The retropharyngeal steroid use during operation on the fusion rate and dysphagia after ACDF? A systematic review and meta-analysis. *European Spine Journal*. 2022;31(2):288-300. doi:10.1007/S00586-021-06727-1/METRICS
53. Siasios I, Fountas K, Dimopoulos V, Pollina J. The role of steroid administration in the management of dysphagia in anterior cervical procedures. *Neurosurg Rev*. 2018;41(1):47-53. doi:10.1007/S10143-016-0741-8/METRICS
54. Edwards CC, Heller JG, Murakami H. Corpectomy Versus Laminoplasty for Multilevel Cervical Myelopathy. *Spine (Phila Pa 1976)*. 2002;27(11):1168-1175. doi:10.1097/00007632-200206010-00007
55. Chen Z, Wei X, Li F, et al. Tracheal Traction Exercise Reduces the Occurrence of Postoperative Dysphagia After Anterior Cervical Spine Surgery. *Spine (Phila Pa 1976)*. 2012;37(15):1292-1296. doi:10.1097/BRS.0b013e3182477f26
56. Smith-Hammond CA, New KC, Pietrobon R, Curtis DJ, Scharver CH, Turner DA. Prospective Analysis of Incidence and Risk Factors of Dysphagia in Spine Surgery Patients. *Spine (Phila Pa 1976)*. 2004;29(13):1441-1446. doi:10.1097/01.BRS.0000129100.59913.EA

57. Miles A, Jamieson G, Shasha L, Davis K. Characterizing dysphagia after spinal surgery. *J Spinal Cord Med*. 2021;44(5):733-741. doi:10.1080/10790268.2019.1665613
58. Logemann JA, Pauloski BR, Rademaker AW, et al. Swallowing disorders in the first year after radiation and chemoradiation. *Head Neck*. 2008;30(2):148-158. doi:10.1002/hed.20672
59. Ko JH, Han KS, Yoon SJ. Efficacy of Laryngeal Rehabilitation Therapy on Dysphagia after Anterior Cervical Surgery: Prospective, Randomized Control Trial. *J Clin Med*. 2022;11(9):2470. doi:10.3390/jcm11092470
60. Tait RC, Zoberi K, Ferguson M, et al. Persistent Post-Mastectomy Pain: Risk Factors and Current Approaches to Treatment. *J Pain*. 2018;19(12):1367-1383. doi:10.1016/j.jpain.2018.06.002
61. Chappell AG, Bai J, Yuksel S, Ellis MF. Post-Mastectomy Pain Syndrome: Defining Perioperative Etiologies to Guide New Methods of Prevention for Plastic Surgeons. Published online 2020.
62. de Menezes Couceiro TC, Valença MM, Raposo MCF, de Orange FA, Amorim MMR. Prevalence of Post-Mastectomy Pain Syndrome and Associated Risk Factors: A Cross-Sectional Cohort Study. *Pain Management Nursing*. 2014;15(4):731-737. doi:10.1016/j.pmn.2013.07.011
63. Bruce J, Thornton AJ, Scott NW, et al. Chronic preoperative pain and psychological robustness predict acute postoperative pain outcomes after surgery for breast cancer. *Br J Cancer*. 2012;107(6):937-946. doi:10.1038/bjc.2012.341
64. Bruce J, Thornton AJ, Powell R, et al. Psychological, surgical, and sociodemographic predictors of pain outcomes after breast cancer surgery: A population-based cohort study. *Pain*. 2014;155(2):232-243. doi:10.1016/j.pain.2013.09.028
65. DeSantis CE, Ma J, Goding Sauer A, Newman LA, Jemal A. Breast cancer statistics, 2017, racial disparity in mortality by state. *CA Cancer J Clin*. 2017;67(6):439-448. doi:10.3322/caac.21412
66. Allemani C, Weir HK, Carreira H, et al. Global surveillance of cancer survival 1995–2009: analysis of individual data for 25 676 887 patients from 279 population-based registries in 67 countries (CONCORD-2). *The Lancet*. 2015;385(9972):977-1010. doi:10.1016/S0140-6736(14)62038-9
67. Schug SA, Pogatzki-Zahn EM. Chronic pain after surgery or injury. *Pain Clin Updates*. 2011;19(1):1-4.
68. Stubblefield MD, Custodio CM. Upper-Extremity Pain Disorders in Breast Cancer. *Arch Phys Med Rehabil*. 2006;87(3):96-99. doi:10.1016/j.apmr.2005.12.017
69. Amichetti M, Caffo O. Pain after quadrantectomy and radiotherapy for early-stage breast cancer: incidence, characteristics and influence on quality of life. Published online 2003.
70. Wallace AM, Wallace MS. Postmastectomy and postthoracotomy pain. *Anesthesiol Clin North Am*. 1997;15(2):353-370.
71. Shamley D, Lascurain-Aguirrebeña I, Oskrochi R, Srinaganathan R. Shoulder morbidity after treatment for breast cancer is bilateral and greater after mastectomy. *Acta Oncol (Madr)*. 2012;51(8):1045-1053. doi:10.3109/0284186X.2012.695087
72. Shamley D, Srinaganathan R, Oskrochi R, Lascurain-Aguirrebeña I, Sugden E. Three-dimensional scapulothoracic motion following treatment for breast cancer. *Breast Cancer Res Treat*. 2009;118(2):315-322. doi:10.1007/s10549-008-0240-x
73. Engel J, Kerr J, Schlesinger-raab A, Eckel R, Sauer H, Hölzel D. Predictors of Quality of Life of Breast Cancer Patients. *Acta Oncol (Madr)*. 2003;42(7):710-718. doi:10.1080/02841860310017658
74. Esteban-Simón A, Díez-Fernández DM, Artés-Rodríguez E, et al. Absolute and Relative Handgrip Strength as Indicators of Self-Reported Physical Function and Quality of Life in Breast Cancer Survivors: The EFICAN Study. *Cancers (Basel)*. 2021;13(21):5292. doi:10.3390/cancers13215292
75. Kwan W, Jackson J, Weir LM, Dingee C, McGregor G, Olivotto IA. Chronic Arm Morbidity After Curative Breast Cancer Treatment: Prevalence and Impact on Quality of Life. *Journal of Clinical Oncology*. 2002;20(20):4242-4248. doi:10.1200/JCO.2002.09.018
76. Hayes SC, Rye S, Battistutta D, DiSipio T, Newman B. Upper-body morbidity following breast cancer treatment is common, may persist longer-term and adversely influences quality of life. *Health Qual Life Outcomes*. 2010;8(1):92. doi:10.1186/1477-7525-8-92
77. Wisotzky E, Hanrahan N, Lione TP, Maltser S. Deconstructing Postmastectomy Syndrome. *Phys Med Rehabil Clin N Am*. 2017;28(1):153-169. doi:10.1016/j.pmr.2016.09.003

78. Garssen B, Boomsma MF, de Jager Meezenbroek E, et al. Stress management training for breast cancer surgery patients. *Psychooncology*. 2013;22(3):572-580. doi:10.1002/pon.3034
79. Lacroix C, Duhoux FP, Bettendorff J, et al. Impact of Perioperative Hypnosedation on Postmastectomy Chronic Pain: Preliminary Results. *Integr Cancer Ther*. 2019;18:153473541986949. doi:10.1177/1534735419869494
80. De Groef A, Van Kampen M, Vervloesem N, et al. Myofascial techniques have no additional beneficial effects to a standard physical therapy programme for upper limb pain after breast cancer surgery: a randomized controlled trial. *Clin Rehabil*. 2017;31(12):1625-1635. doi:10.1177/0269215517708605
81. Ammitzbøll G, Andersen KG, Bidstrup PE, et al. Effect of progressive resistance training on persistent pain after axillary dissection in breast cancer: a randomized controlled trial. *Breast Cancer Res Treat*. 2020;179(1):173-183. doi:10.1007/s10549-019-05461-z
82. Heijnen BJ, Speyer R, Kertscher B, et al. Dysphagia, Speech, Voice, and Trismus following Radiotherapy and/or Chemotherapy in Patients with Head and Neck Carcinoma: Review of the Literature. *Biomed Res Int*. 2016;2016:1-24. doi:10.1155/2016/6086894
83. Sanguineti G, Pai S, Agbahiwe H, et al. HPV-related oropharyngeal carcinoma with Overt Level II and/or III metastases at presentation: The risk of subclinical disease in ipsilateral levels IB, IV and V. *Acta Oncol (Madr)*. 2014;53(5):662-668. doi:10.3109/0284186X.2013.858825
84. Van Dyne EA, Henley SJ, Saraiya M, Thomas CC, Markowitz LE, Benard VB. Trends in Human Papillomavirus–Associated Cancers — United States, 1999–2015. *MMWR Morb Mortal Wkly Rep*. 2018;67(33):918-924. doi:10.15585/mmwr.mm6733a2
85. Chaturvedi AK, Engels EA, Anderson WF, Gillison ML. Incidence Trends for Human Papillomavirus–Related and –Unrelated Oral Squamous Cell Carcinomas in the United States. *Journal of Clinical Oncology*. 2008;26(4):612-619. doi:10.1200/JCO.2007.14.1713
86. Gillison ML, Chaturvedi AK, Anderson WF, Fakhry C. Epidemiology of Human Papillomavirus–Positive Head and Neck Squamous Cell Carcinoma. *Journal of Clinical Oncology*. 2015;33(29):3235-3242. doi:10.1200/JCO.2015.61.6995
87. Tseng BP, Giedzinski E, Izadi A, et al. Functional Consequences of Radiation-Induced Oxidative Stress in Cultured Neural Stem Cells and the Brain Exposed to Charged Particle Irradiation. *Antioxid Redox Signal*. 2014;20(9):1410-1422. doi:10.1089/ars.2012.5134
88. Jiang J, Li Y, Shen Q, et al. Effect of Pregabalin on Radiotherapy-Related Neuropathic Pain in Patients With Head and Neck Cancer: A Randomized Controlled Trial. *Journal of Clinical Oncology*. 2019;37(2):135-143. doi:10.1200/JCO.18.00896
89. Azzam P, Mroueh M, Francis M, Abou Daher A, Zeidan YH. Radiation-induced neuropathies in head and neck cancer: prevention and treatment modalities. *Ecancermedicalscience*. 2020;14. doi:10.3332/ecancer.2020.1133
90. Delanian S, Lefaix JL, Pradat PF. Radiation-induced neuropathy in cancer survivors. *Radiotherapy and Oncology*. 2012;105(3):273-282. doi:10.1016/j.radonc.2012.10.012
91. King SN, Dunlap NE, Tennant PA, Pitts T. Pathophysiology of Radiation-Induced Dysphagia in Head and Neck Cancer. *Dysphagia*. 2016;31(3):339-351. doi:10.1007/s00455-016-9710-1
92. Hutcheson KA, Lewin JS, Barringer DA, et al. Late dysphagia after radiotherapy-based treatment of head and neck cancer. *Cancer*. 2012;118(23):5793-5799. doi:10.1002/cncr.27631
93. Forastiere AA, Goepfert H, Maor M, et al. Concurrent Chemotherapy and Radiotherapy for Organ Preservation in Advanced Laryngeal Cancer. *New England Journal of Medicine*. 2003;349(22):2091-2098. doi:10.1056/NEJMoa031317
94. Mehta PS, Harrison LB. Function and organ preservation in adult cancers of the head and neck. *Expert Rev Anticancer Ther*. 2007;7(3):361-371. doi:10.1586/14737140.7.3.361
95. Harrison LB, Ferlito A, Shaha AR, Bradley PJ, Genden EM, Rinaldo A. Current philosophy on the management of cancer of the base of the tongue. *Oral Oncol*. 2003;39(2):101-105. doi:10.1016/S1368-8375(02)00048-9
96. Carrara-de Angelis E, Feher O, Barros APB, Nishimoto IN, Kowalski LP. Voice and Swallowing in Patients Enrolled in a Larynx Preservation Trial. *Arch Otolaryngol Head Neck Surg*. 2003;129(7):733. doi:10.1001/archotol.129.7.733

97. Nguyen NP, Moltz CC, Frank C, et al. Long-Term Aspiration following Treatment for Head and Neck Cancer. *Oncology*. 2008;74(1-2):25-30. doi:10.1159/000138976
98. Lazarus C, Logemann JA, Pauloski BR, et al. Effects of radiotherapy with or without chemotherapy on tongue strength and swallowing in patients with oral cancer. *Head Neck*. 2007;29(7):632-637. doi:10.1002/hed.20577
99. Lazarus CL, Logemann JA, Pauloski BR, et al. Swallowing and Tongue Function Following Treatment for Oral and Oropharyngeal Cancer. *Journal of Speech, Language, and Hearing Research*. 2000;43(4):1011-1023. doi:10.1044/jslhr.4304.1011
100. Hagenacker T, Bude V, Naegel S, et al. Patient-conducted anodal transcranial direct current stimulation of the motor cortex alleviates pain in trigeminal neuralgia. *J Headache Pain*. 2014;15(1):78. doi:10.1186/1129-2377-15-78
101. Hosomi K, Shimokawa T, Ikoma K, et al. Daily repetitive transcranial magnetic stimulation of primary motor cortex for neuropathic pain: A randomized, multicenter, double-blind, crossover, sham-controlled trial. *Pain*. 2013;154(7):1065-1072. doi:10.1016/j.pain.2013.03.016
102. Radic JAE, Beauprie I, Chiasson P, Kiss ZHT, Brownstone RM. Motor Cortex Stimulation for Neuropathic Pain: A Randomized Cross-over Trial. *Canadian Journal of Neurological Sciences / Journal Canadien des Sciences Neurologiques*. 2015;42(6):401-409. doi:10.1017/cjn.2015.292
103. Ngernyam N, Jensen MP, Arayawichanon P, et al. The effects of transcranial direct current stimulation in patients with neuropathic pain from spinal cord injury. *Clinical Neurophysiology*. 2015;126(2):382-390. doi:10.1016/j.clinph.2014.05.034
104. Ludlow CL. Electrical neuromuscular stimulation in dysphagia: current status. *Curr Opin Otolaryngol Head Neck Surg*. 2010;18(3):159-164. doi:10.1097/MOO.0b013e3283395dec
105. Suiter DM, Leder SB, Ruark JL. Effects of Neuromuscular Electrical Stimulation on Submental Muscle Activity. *Dysphagia*. 2006;21(1):56-60. doi:10.1007/s00455-005-9010-7
106. Ludlow CL, Humbert I, Saxon K, Poletto C, Sonies B, Crujido L. Effects of Surface Electrical Stimulation Both at Rest and During Swallowing in Chronic Pharyngeal Dysphagia. *Dysphagia*. 2007;22(1):1-10. doi:10.1007/s00455-006-9029-4
107. Humbert IA, Poletto CJ, Saxon KG, et al. The effect of surface electrical stimulation on hyolaryngeal movement in normal individuals at rest and during swallowing. *J Appl Physiol*. 2006;101(6):1657-1663. doi:10.1152/japplphysiol.00348.2006
108. Ryu JS, Kang JY, Park JY, et al. The effect of electrical stimulation therapy on dysphagia following treatment for head and neck cancer. *Oral Oncol*. 2009;45(8):665-668. doi:10.1016/j.oraloncology.2008.10.005
109. Lin PH, Hsiao TY, Chang YC, et al. Effects of functional electrical stimulation on dysphagia caused by radiation therapy in patients with nasopharyngeal carcinoma. *Supportive Care in Cancer*. 2011;19(1):91-99. doi:10.1007/s00520-009-0792-2
110. Langmore SE, McCulloch TM, Krisciunas GP, et al. Efficacy of electrical stimulation and exercise for dysphagia in patients with head and neck cancer: A randomized clinical trial. *Head Neck*. 2016;38(S1). doi:10.1002/hed.24197
111. Papageorgiou TD, Lisinski JM, McHenry MA, White JP, LaConte SM. Brain–computer interfaces increase whole-brain signal to noise. *Proceedings of the National Academy of Sciences*. 2013;110(33):13630-13635. doi:10.1073/pnas.1210738110
112. Giahi Saravani A, Forseth KJ, Tandon N, Pitkow X. Dynamic Brain Interactions during Picture Naming. *eNeuro*. 2019;6(4):ENEURO.0472-18.2019. doi:10.1523/ENEURO.0472-18.2019